NATIONAL ADVISORY COMMITTEE FOR AERONAUTICS

TECHNICAL NOTE 2407

METHOD OF ANALYSIS FOR COMPRESSIBLE FLOW PAST ARBITRARY TURBOMACHINE BLADES ON GENERAL SURFACE OF REVOLUTION

By Chung-Hua Wu and Curtis A. Brown

Lewis Flight Propulsion Laboratory
Cleveland, Ohio

Washington

July 1951

NATIONAL ADVISORY COMMITTEE FOR AERONAUTICS

TECHNICAL NOTE 2407

METHOD OF ANALYSIS FOR COMPRESSIBLE FLOW PAST ARBITRARY TURBOMACHINE BLADES ON GENERAL SURFACE OF REVOLUTION

By Chung-Hua Wu and Curtis A. Brown

SUMMARY

A method of obtaining the flow of a nonviscous compressible fluid past arbitrary compressor or turbine blades between two neighboring surfaces of revolution is presented. The equations of continuity and motion obtained for such flow are combined into a nonlinear second-order differential equation in terms of a stream function defined for such flow. Numerical solution by the use of differentiation coefficients for unequally spaced grid points is suggested. Means for satisfying the boundary conditions outside the channel and solutions by the relaxation method with manual computation and by a matrix method with a large-scale digital computing machine are described.

Satisfactory results were obtained by the method described in the investigation of the detailed flow variation of a compressible fluid past typical high-solidity, highly cambered thick turbine blades on a cylindrical surface. The variations in fluid properties across the channel appeared to be representable by a second-degree function. The mean streamline approximately followed the shape of the mean channel line of the cascade and had lower curvature. The variation of specific mass flow along the mean streamline followed the trend of the variation in the channel width. In general, the variation in specific mass flow was significantly higher than that given by the ratio in channel width and the effect extended outside the channel. The velocity distribution around the blade obtained in the theoretical calculation compares very well with experimental values.

INTRODUCTION

A basic aerodynamic problem of turbojet and turbine-propeller engines is the flow of compressible fluid past a series of blades in circular arrangement. In axial-flow type turbomachines, if the blades are relatively short in the radial dimension and are bounded by cylindrical walls, the theoretical flow passing through the blades is usually computed on the basis of two-dimensional flow on a cylindrical surface,

which is then developed into a plane for convenience of calculation. A number of methods have been proposed to obtain the theoretical flow through such a given cascade of airfoils, including analytical methods using conformal mapping, interference technique, and Prandtl-Glauert or Chaplygin-Kármán-Tsien approximation for compressible flow (references 1 to 6), graphical procedure (references 7 to 10), and other mechanical and electrical devices (reference 10). For radial- and mixed-flow type turbomachines, the available methods consider incompressible flow in a radial plane (references 7 and 11 to 16) or compressible flow on a conical surface (reference 17). However, in current axial-flow turbomachines, the hub and casing walls may be either tapered or curved, which causes the fluid to flow on a noncylindrical surface; and in centrifugal machines, the flow surfaces are usually quite curved toward the inlet (see fig. 1). A method of analysis is therefore developed at the NACA Lewis laboratory to analyze the two-dimensional compressible flow for the fluid between two neighboring surfaces of revolution in these turbomachines (fig. 1). The equations of continuity and motion for irrotational absolute flow are first obtained for such flows and are then combined into a nonlinear second-order partial differential equation. Because the change of fluid properties passing through turbomachine blades is, in general, large and the shapes of surface and blades are arbitrary, numerical solution by the finite-difference approach is suggested.

Solving the flow through a cascade of blades of arbitrary camber and thickness by the finite-difference method involves two main difficulties: (1) the curved boundaries formed by the blade surface, and (2) the large number of grid points necessary to cover the whole flow region. The first difficulty is removed by the recently available differentiation formula and coefficients for unequally spaced grid points (reference 18). With these formulas and coefficients, the curved boundary can be handled in the same manner as a straight boundary. The second difficulty can be reduced by the use of higher-degree polynomial representations (references 18 and 19). Furthermore, if a modern high-speed large-scale digital machine is available, the set of simultaneous difference equations in the stream function can be very quickly solved by the matrix process given in reference 18, and consequently, successively improved solutions for compressible flow can be obtained in a reasonably short time. Without such a machine, it is desirable to obtain an approximate solution for compressible flow by either graphic, mechanical, or other approximate methods and to use the relaxation method (references 20 and 21) for the final improvements.

In turbomachines with a relatively large radial dimension, curved hub and casing walls, or if designed on velocity diagrams other than the free-vortex type, the radial flow assumes primary importance. For such

turbomachines, methods of flow analysis have been proposed that take into account the radial flow but consider only the variation of the fluid properties on a mean stream surface passing between two blades (reference 22). When applying such methods of analysis to turbomachines with thick blades, it is necessary to have some knowledge of the effect of area reduction due to blade thickness on the mean flow and the relation between the blade shape and the shape of the mean streamline at various radii. For this reason, the method developed is applied to investigate the detailed compressible flow in a typical turbine cascade with highly cambered thick blades. The theoretical velocity on the blade is compared with experimental data obtained at the NACA Lewis laboratory.

SYMBOLS

The following symbols are used in this report:

a,b,c	points on streamline
B	differentiation coefficients
C	constant
E	error
H	total enthalpy based on absolute velocity
h	static enthalpy
I	$h + \frac{1}{2} W^2 - \frac{1}{2} \omega^2 r^2$
L	blade length projected on z-axis
l,φ	orthogonal coordinates on mean surface of revolution, (fig. 1)
M	total mass flow passing through space between two neighboring blades
n	degree of polynomial
P	pitch or spacing
p	static pressure
r	radial distance from the axis of machine, (fig. 1)

t	blade thickness in pitch direction
W	velocity relative to blade
y	$r\varphi$
z	distance along axis of machine, (fig. 1)
α	flow angle in $l\varphi$-plane, $\tan^{-1}\frac{1}{r}\frac{W\varphi}{W_l}$
γ	ratio of specific heats
δ	grid spacing
ρ	mass density
σ	$\tan^{-1}\frac{W_r}{W_z}$, (fig. 1)
τ	normal thickness of stream filament of revolution, (fig. 1)
ψ	stream function
ω	angular velocity of blade

Subscripts:

i	inlet
j,k	grid points where differentiation coefficients are applied
l,φ	meridional and circumferential component, (fig. 1)
m	mean streamline
n	degree of polynomial
p	pressure surface
s	suction surface
T	total, or stagnation, state

Superscripts:

a,b,c, . . . i,j,k	grid points
1,2	indicate first and second derivatives, respectively

METHOD OF SOLUTION

The steady isentropic flow of a nonviscous compressible fluid along a stream filament of revolution described by the orthogonal coordinates l and φ on the mean surface of revolution and a varying normal thickness of the filament τ (fig. 1) is governed by the following equations of continuity and irrotational absolute flow and the isentropic pressure-density relation (see appendix for derivation of the first two equations):

$$\frac{\partial(\tau \rho W_l r)}{\partial l} + \frac{\partial(\tau \rho W_\varphi)}{\partial \varphi} = 0 \tag{1}$$

$$\frac{\partial W_\varphi}{\partial l} - \frac{1}{r}\frac{\partial W_l}{\partial \varphi} + \frac{W_\varphi \sin \sigma}{r} + 2\omega \sin \sigma = 0 \tag{2}$$

$$p = C \rho^\gamma \tag{3}$$

From equation (1), a stream function ψ can be defined by the following relations:

$$\left.\begin{aligned} \tau \rho W_l r &= \frac{\partial \psi}{\partial \varphi} \\ \tau \rho W_\varphi &= -\frac{\partial \psi}{\partial l} \end{aligned}\right\} \tag{4}$$

Substituting equations (4) in equation (2) results in

$$\frac{\partial^2 \psi}{\partial l^2} + \left(\frac{\sin \sigma}{r} - \frac{\partial \ln \tau}{\partial l}\right)\frac{\partial \psi}{\partial l} + \frac{1}{r^2}\frac{\partial^2 \psi}{\partial \varphi^2} -$$

$$\left(\frac{\partial \ln \rho}{\partial l}\frac{\partial \psi}{\partial l} + \frac{1}{r^2}\frac{\partial \ln \rho}{\partial \varphi}\frac{\partial \psi}{\partial \varphi} + 2\omega \tau \rho \sin \sigma\right) = 0 \tag{5}$$

In the numerical solution of the problem, iteration is necessary for compressible flow. A network of grid points is chosen to cover the whole flow region, and finite-difference equations are obtained for the first three terms of equation (5). The last term is taken as constant during the solution of the ψ values and recomputed from the improved values of ψ for the next solution (references 20 and 21). In this way, the numerical coefficients at each grid point are determined by the geometry of the problem alone.

The value of density is most conveniently expressed throughout the flow region in terms of velocity and enthalpy by the use of equation (3) and the relation for a perfect gas:

$$\frac{\rho}{\rho_{T,i}} = \left(\frac{h}{H_i}\right)^{\frac{1}{\gamma-1}} = \left(\frac{I + \frac{1}{2}\omega^2 r^2 - \frac{1}{2}W^2}{H_i}\right)^{\frac{1}{\gamma-1}} \tag{6}$$

where I is constant throughout the flow region for adiabatic, absolutely irrotational, and steady relative flow (reference 22). (For application to stator blades, ω becomes zero, W becomes the absolute velocity, and I becomes H.) If the components of W as expressed by equations (4) are substituted in equation (6), the following equation is

$$\frac{\rho}{\rho_{T,i}} = \left[\frac{I + \frac{1}{2}\omega^2 r^2}{H_i} - \frac{\left(\frac{\partial\psi}{\partial l}\right)^2 + \frac{1}{r^2}\left(\frac{\partial\psi}{\partial\varphi}\right)^2}{2 H_i \tau^2 \rho^2}\right]^{\frac{1}{\gamma-1}} \tag{7}$$

In order to facilitate the evaluation of the density from the ψ-derivatives, equation (7) can be rewritten in the following form:

$$\Sigma = (1 - \Phi/\Sigma)^{\frac{2}{\gamma-1}} \tag{7a}$$

where

$$\Sigma = \left(\frac{\rho}{\rho_{T,i}}\right)^2 \left(\frac{I + \frac{1}{2}\omega^2 r^2}{H_i}\right)^{-\frac{2}{\gamma-1}} \tag{7b}$$

and

$$\Phi = \left[\left(\frac{\partial\psi}{\partial l}\right)^2 + \frac{1}{r^2}\left(\frac{\partial\psi}{\partial\varphi}\right)^2\right]\left[2(\tau\,\rho_{T,i})^2\,H_i\right]^{-1}\left(\frac{I + \frac{1}{2}\omega^2r^2}{H_i}\right)^{-\frac{\gamma+1}{\gamma-1}} \tag{7c}$$

With the relation between ρ and ψ-derivatives in this form, either a table may be constructed by computing Σ for equally spaced values of Φ through iteration on a punch card machine, or a graph may be constructed by computing Φ for a number of Σ. Because $\rho_{T,i}$, H_i, I, ω, r, and τ are all known values, with the aid of the table or graph, the value of density at any point can be easily obtained after the first-order derivatives of ψ are computed by using the differential coefficients for equally and unequally spaced grid points given in references 23 and 18, respectively.

The first-order derivatives of density are then computed and combined with the first-order derivatives of ψ. If the last term in equation (5) is denoted by J and the differentiation coefficients, which multiply the ψ value at point j to give the second and first derivatives at point i using an n^{th}-degree polynomial, are denoted by ${}^{2}B^{i}_{n\,j}$ and ${}^{1}B^{i}_{n\,j}$, respectively, the finite-difference form of equation (5) at the grid point i can be written as

$$\sum_{j=0}^{n}\left[{}^{2}B^{i}_{n\,j} + \left(\frac{\sin\sigma}{r} - \frac{\partial\ln\tau}{\partial l}\right)^{i}{}^{1}B^{i}_{n\,j}\right]\psi^j + \sum_{k=0}^{n}\frac{{}^{2}B^{i}_{n\,k}}{(r^i)^2}\psi^k + J^i = 0 \tag{8}$$

where ψ^j and ψ^k denote ψ values on the surface along l and φ coordinates, respectively (figs. 1 and 2). If second-degree polynomial representation is chosen $(n=2)$, three points are involved in the numerical differentiation in each direction, and the center-point formula can always be used for all interior grid points. If fourth-degree polynomial representation is chosen $(n=4)$, five points are involved in each direction and the off-center-point formula has to be used at the point next to the boundary. Two typical cases where odd spacings are used in the calculation of the coefficients because of a curved boundary are shown in figure 2. In the case where ψ^i is at $j=2$, $k=2$, the center-point formula is used in both directions, with equal-space l-direction coefficients obtainable from reference 23 and

with φ-direction coefficients for the odd space at the boundary obtainable from reference 18. In the other case where ψ^1 is at $j=2$, $k=3$, again the equal-space center-point coefficients are used in the l-direction; but in the φ-direction an off-center-point formula for coefficients must be used, including an odd space at the boundary, again obtainable from reference 18. It is desirable, where possible, to have the spacing near the boundary somewhat shorter than the regular equal spacing so that accuracy at the point next to the boundary is comparable with that at other points. By using a five-point system, many less grid points are required in comparison with the three-point system for the same accuracy. (See reference 18.) In the present problem, the variation of ψ is only rapid near the leading and trailing edges of the blade and the grid pattern should be determined for these regions first.

After the degree of polynomial representation and the size of grid have been chosen, a finite-difference equation (8) can be easily written for each interior grid point using the differentiation coefficients for equal and unequal grid spacings. The constant ψ value on the suction surface can be arbitrarily chosen and the constant ψ value on the pressure surface is determined by the mass flow passing through the channel or at the inlet as follows:

$$\psi_p - \psi_s = \int_{\varphi_s}^{\varphi_p} \frac{\partial \psi}{\partial \varphi} \, d\varphi = \int_{\varphi_s}^{\varphi_p} \tau \rho W_l r \, d\varphi = M \tag{9}$$

Outside the channel two reference lines, a pitch angle apart, can be drawn either parallel to the l-axis or parallel to the inlet and exit angles in the $l\varphi$-plane. (Parallelism with the inlet and exit angles, as shown in fig. 3, is a little more convenient for the purpose of drawing streamlines after the solution is obtained.) Because the fluid state repeats itself for each pitch angle along the φ-direction, only the grid points lying between the reference lines need to be included in the calculation when the number of grid spaces per pitch angle is an integer, and the central five-point formula can always be used at every grid point between these lines. For example, at grid point c (fig. 3), the ψ values at a and b are obtained in terms of the ψ values at i and j, which are a pitch angle apart from a and b, respectively, by the following relation:

$$\begin{aligned} \psi^a &= \psi^i + (\psi_p - \psi_s) \\ \psi^b &= \psi^j + (\psi_p - \psi_s) \end{aligned} \tag{10}$$

Inlet and Exit Boundary Conditions

The solution of the present problem in terms of ψ has an interesting feature in the boundary conditions. As noted in the previous section, the ψ value is constant along either the suction or pressure surfaces, which are fixed boundaries; and outside the channel, there is no longer a fixed boundary, but there is the condition that the flow repeats itself for every pitch angle in the φ-direction. Sufficiently far upstream of the blade, an inlet station can be chosen so the boundary condition there requires the fluid state to be uniform in the φ-direction and prescribes the inlet angle β_i. The following two methods have been devised to account for this boundary condition:

Fixed-angle method. - A part of the grid system in the $l\varphi$-plane near the inlet station i-i is shown in figure 4(a). In order to write the finite-difference equation at point a, the value of ψ at point c to the left of station i-i can be obtained by using the given inlet angle β_i and the linear variation of ψ at station i-i

$$\psi^c = \psi^d = \psi^a + \frac{\delta_l \tan \alpha_i}{\delta \varphi} (\psi^b - \psi^a)$$

$$= \left(1 - \frac{\delta_l}{\delta \varphi} \tan \alpha_i\right) \psi^a + \left(\frac{\delta_l}{\delta \varphi} \tan \alpha_i\right) \psi^b \qquad (11)$$

The coefficients of ψ^a and ψ^b in equation (11) after having been multiplied by ${}_nB_c^a$ are added to the regular coefficients at points a and b; otherwise the points a and b are treated in the same manner as other interior points. Whether the inlet station i-i is chosen sufficiently far away from the blade is indicated by the linearity of the ψ variation at that station as obtained in the solution.

Streamline-adjustment method. - If the first station i-i is chosen sufficiently far from the blades, the variation of stream function to the left of the station i-i is linear in the circumferential direction. The value of the stream function, however, depends on the inlet angle. If solutions for a range of inlet angles are desired, they can be obtained by specifying a number of linearly varying stream functions to the left of station i-i as fixed boundary values. The streamline obtained in the solution then gives the value of the inlet angle. If, however, the solution for a certain inlet angle is desired, the streamline obtained in the solution must be adjusted according to that inlet

angle, (for example as ab in fig. 4(b) is adjusted to position ac), thereby obtaining an improved set of boundary values of the stream functions to be used in the next calculation. This method is of course not as accurate and convenient as the fixed-angle method for obtaining a solution for a given inlet angle but is desirable in the matrix solution (to be discussed in the following section) because the inlet angle is not involved in the matrix factorization, making the same matrix factors usable for a range of inlet angles and Mach numbers.

At the exit station far downstream of the blade, the same methods can be applied. For a blade having a sharp trailing edge, the Kutta-Joukowski condition can be used and the correct exit angle far downstream is the one that gives the flow at the trailing edge satisfying that condition. For round trailing edges, either the position of the stagnation point can be assumed or some available empirical rules for the exit angle used. If the calculation is made to compare with certain experimental results, the measured exit angle can be used.

Solution of Finite-Difference Equations

With the grid system and the degree of polynomial representation chosen and the boundary conditions taken into account, the problem remaining is the solution of the set of N linear algebraic equations (8) written for N interior grid points. For a small number of solutions with a given blade, the best method is the relaxation method (reference 20). A modification of this method involving the use of higher-order differences is suggested by Fox (reference 18). Formulas and the table of coefficients obtained in reference 18 enable the direct use of higher-degree polynomials for problems with curved boundaries. For the present flow problems, it is necessary to include a large domain to get to the boundary conditions that are given at places far from the blades. The use of higher-degree polynomials will greatly reduce the numerical work.

If a number of cases are to be solved for a given set of blades on a given surface, it is advantageous to solve the problem on a large-scale digital computing machine. If a very high-speed digital machine is available, the simultaneous equation is best solved by Liebmann's iterative process, which is the most simple to set up (reference 24). If only a relatively slow-speed machine is available, the matrix process suggested in reference 18 is most suitable.

Matrix solution. - In the matrix solution, the entire equation (8) is used with ρ being kept constant during any one cycle. Several cycles are necessary for compressible flow because ρ is in a continual process of change during each calculation according to equation (7). The matrix method is found most satisfactory when several solutions are required for a given blading configuration, (for instance, in the case where the flow is to be determined through a blading at several inlet Mach numbers or inlet angles) because the factorization of the matrix is the most time-consuming part of the problem and once completed the matrix may be used again and again as one of the inlet flow conditions is varied. For example, in a problem similar to the cascade problem in which 400 grid points and fourth-degree polynomials were used, it took about 60 hours to factorize the matrix on an IBM Card Programmed Electronic Calculator, and solving the set of values of ψ at all grid points for a given set of J values only takes 2 hours. The rounding-off error is found to be very small.

Relaxation solution. - In the relaxation solution, the entire equation (8) is used in the calculation of the residuals; but only the first two terms are used in the actual relaxation. As in the matrix solution, several cycles are required for compressible flow because ρ is not allowed to vary during the relaxation process whereas actually ρ is changing according to equation (7). Consequently, after each cycle new values of ρ are calculated and used in the determination of an improved J as in the matrix method.

Iteration method of Liebmann. - The iteration method of Liebmann is simplest to set up on a digital computing machine; but it is the slowest method, and therefore it can only be used for the present problem on a high-speed machine. The boundary conditions and the between-cycles J correction process are the same as those in the matrix and relaxation methods.

ACCURACY OF FINAL RESULTS

Several factors affect the accuracy of the final results: the degree of Lagrangian polynomial used, the size relative to the airfoil of the network spacings, the smallness to which the residuals are reduced, and the number of cycles carried out for compressible flow.

The fourth-degree Lagrangian polynomial has been found to be the most applicable to the type of calculation under consideration. The use of a second-degree polynomial, in general, requires a smaller grid spacing, necessitating a much larger number of network points than

the fourth-degree polynomial. Polynomials of higher degree than the fourth are not desirable within the channel, because fitting the points necessary for these higher-degree polynomials circumferentially inside the channel may require a smaller grid spacing. Also the accuracy near the leading and trailing edges of the blade is best obtained by using small spacing. Outside the channel, however, the use of a higher-degree polynomial would not only reduce the amount of work but also would specify more completely the condition that the flow repeats circumferentially every pitch angle.

Formulas that can be used, after the problem has been completed, to determine the order of magnitude of the error at any point are given in references 18 and 23. These formulas give only qualitative information concerning the obtainable accuracy for the grid size and the degree of polynomial chosen, especially when there is no solution of a similar problem available. Because no solution is available with which to apply these formulas at the start of the example to be discussed in the following section, a somewhat smaller grid spacing than that required for the use of a fourth-degree polynomial across the channel is chosen. (See fig. 3.) Results obtained in that example indicate that the grid chosen gives sufficient accuracy for the present purpose. If a more accurate result is desired around the nose or tail region, either small spacing can be used in these regions or the flow in these regions can be improved by using a finer net after the solution is obtained with the original coarse net.

For the matrix and iteration methods, the final accuracy is determined by the choice of grid size and degree of polynomial; for the relaxation method, however, the degree of residual reduction must also be included in an accuracy determination. The smallness to which the residuals can be reduced depends essentially on the amount of labor put into the problem; but the smallness may be limited by the use of too large grid spaces or too low a degree of polynomial. An approximate method for estimating, at the beginning of the problem, the degree of residual reduction necessary is outlined as follows: It is assumed that an error of 1 percent in addition to that introduced by the finite-difference equations will be tolerated in the first order derivatives of ψ. For example, the following equation can be written in the φ-direction by the use of the usual differentiation formula:

$$\left(\frac{d\psi}{\partial l}\right)_d = \frac{(\psi^c + E^c) - (\psi^e + E^e)}{2\delta\varphi} \tag{12}$$

where the ψ's are the correct values of ψ, the E's are the magnitudes of the errors in ψ, δ_φ is the grid spacing in the φ-direction, and the superscripts c, d, and e refer to three equally spaced grid points (fig. 3). Equation (12) may be rewritten as

$$\left(\frac{\partial\psi}{\partial\varphi}\right)_d = \frac{\psi^c - \psi^e}{2\delta_\varphi} + \frac{E^c - E^e}{2\delta_\varphi} \tag{13}$$

where, in this case, $\frac{E^c - E^e}{2\delta_\varphi}$ is less than 1 percent of $\frac{\psi^c - \psi^e}{2\delta_\varphi}$ as specified. As an example, take $\psi^c - \psi^e$ equal to 1000, then $E^c - E^e < 10$. Because a constant magnitude error is maintained throughout any one area in the network, $|E^c| = |E^e| < 5$. The final residual must be such that a change of ψ of no more than 5 is necessary to reduce the value of the residual to zero. The absolute value of the residual can therefore be no greater than the absolute value of 5 times the relaxation coefficient at the point in question when the final accuracy is reached. For relatively small grid spacings, this method should give a good estimate of the magnitude of allowable residual. Because the relaxation coefficient at the point in question varies from point to point, it is advisable to place the corresponding maximum allowable residuals on the relaxation sheet for ready reference.

NUMERICAL EXAMPLE

The method described is applied to analyze the detailed flow past turbine blades on a cylindrical surface as shown in figure 3. In such a case, σ equals 0, l becomes z, and it is more convenient to use a distance on the circumference $y(=r\varphi)$ instead of the angular coordinate φ (the reduced equations are given in the appendix). Because only one incompressible and one compressible solution were to be obtained at the design condition, the finite-difference equations were solved by the relaxation technique. This particular cascade was chosen because of the relatively high turning and the considerable thickness of the blade involved, thus giving the method described a thorough test. Experimental data for several inlet Mach numbers are available for this cascade, increasing its value as a problem choice. The pitch and axial chord of the cascade are 1.017 and 1.5 inches, respectively.

The grid, shown superposed on the cascade in figure 3, was obtained by dividing the pitch into eight equal parts, thereby arriving at a grid spacing of 0.1271 inch, which is used in both y and z directions. As suggested, fourth-degree Lagrangian polynomials were used throughout the domain to obtain the finite-difference equations.

The reference lines outside the channel were drawn parallel to the flow at the inlet and the exit. The inlet angle is given as $41^\circ 18'$.

The exit angle, as computed by the measured pressure far downstream and the continuity equation, is equal to $-52^{\circ}57'$, which checks quite well with the inverse-sine empirical rule. The fixed-angle method was used to account for the inlet and exit boundary condition. The inlet and exit boundaries were placed a distance equal to $1\frac{1}{2}$ times the pitch from the cascade channel, which was found to be more than sufficient.

The results obtained from the relaxation solution of this cascade serve a threefold purpose: (1) They show the usefulness of the method discussed; (2) they give some detailed information concerning the variation of flow in a two-dimensional cascade that may serve as a basis for devising some simple, good approximate methods of analysis; and (3) they give some useful information for the through-flow analysis in turbines having thick blades.

The results obtained in the incompressible solution are shown in figures 5 to 13. The variations of the magnitudes of W_z, W_y, and W across the channel are shown in figures 5 to 7. The variation in W_y is seen to be larger than that in W_z and larger at the leading portion of the channel than at the trailing portion of the channel. The variation of the velocity components across the channel can be accurately represented by a second-degree function in the y-direction.

Several streamlines, with equal mass flow between them, are shown in figure 8. Also shown is the mean channel line and the mean camber line. The mean streamline, which divides the mass flow in the channel, is seen to have a curvature less than either the mean channel line or the mean camber line and is closer to the suction surface than the pressure surface. (The mean camber line has the highest curvature.) The slope of the mean streamline is compared with those of the blade mean camber line and the mean channel line in figure 9. Inside the channel the absolute value of the mean streamline slope is found to be lower than those of the mean camber and mean channel lines. Proceeding outward from the inlet channel proper the mean streamline slope at first increases above and then approaches the specified inlet and exit values. Figure 9 shows that the specified values are reached approximately one pitch distance from the blade.

The variations of the mean streamline velocity components and their derivatives with respect to z are shown in figures 10 to 13. In figure 10, the variation of W_z along the mean streamline is compared with the variation in channel width. Inside the channel, the increase in W_z due to reduction in channel width is on the average about 4 percent higher than that given by the one-dimensional calculation based on the reduction of the channel width. The difference is due to the nonlinear

variation of W_z across the channel. The influence of the blade thickness also extends a short distance both upstream and downstream of the channel. With a finite blade thickness and a finite blade spacing, the tangential velocity on the mean streamline (fig. 12) is seen to rise above its inlet value in front of the leading edge, to decrease rapidly for the first half of the channel, and then to decrease slowly to a value below its exit value for a short distance downstream of the trailing edge. The derivative with respect to z of the tangential velocity is shown in figure 13.

The compressible solution is obtained for an inlet Mach number of 0.42 in order to compare it with the available experimental data at that inlet Mach number. The results obtained (figs. 14 to 23) are presented in the same manner as those for the incompressible case. The velocities (figs. 14 to 16) show a somewhat higher rate of variation across the channel and can again be approximated by second-degree functions.

The difference in streamlines between the compressible (fig. 17) and the incompressible (fig. 8) solutions is appreciable. In general, the streamlines are pushed farther away from the suction surface. As a result, the mean streamline now approximates the position of the mean channel line better than in the incompressible case but still has a significantly lower curvature.

The comparison between the slope of the mean streamline and those of the mean camber line and the mean channel line in the compressible case (fig. 18) is similar to that in the incompressible case (fig. 9). Instead of the axial velocity in the incompressible case, the specific mass flow ρW_z on the mean streamline is compared with the channel width in the pitch direction in figure 19. The comparison is similar although the difference is somewhat greater in the compressible case. The tangential velocity on the mean streamline obtained in the compressible solution (fig. 20) and its derivative (fig. 21) are again similar to the corresponding curves obtained in the incompressible solution.

The velocity obtained around the blade in the compressible solution is compared in figure 22 with the experimental data obtained at the NACA Lewis laboratory. The agreement is better at the pressure surface than at the suction surface, as might be expected, and is satisfactory as a whole. Constant Mach number contours obtained in the relaxation solution are shown in figure 23. With an inlet Mach number of 0.42 and exit Mach number of 0.55, the variation of Mach number from the pressure surface to the suction surface is quite large. The maximum Mach number on the suction surface exceeds 0.8.

SUMMARY OF RESULTS

A method of obtaining the flow of a nonviscous compressible fluid past arbitrary compressor or turbine blades between two surfaces of revolution is presented. The equations of continuity and motion obtained for such flow are combined into a nonlinear second-order partial differential equation in terms of a stream function defined for such flow. Numerical solution by the use of differentiation coefficients for unequally spaced grid points is suggested. Means for satisfying the boundary conditions outside the channel and solutions by the relaxation method with manual computation and by a matrix method with a large-scale digital computing machine are described.

Satisfactory results were obtained by the method described in the investigation of the detailed flow variation of a compressible fluid past typical high-solidity highly cambered thick turbine blades on a cylindrical surface. The variations in fluid properties across the channel appeared to be representable by a second-degree function. The mean streamline approximately followed the shape of the mean channel line of the cascade and had lower curvature. The variation of specific mass flow along the mean streamline followed the trend of the variation in the channel width. In general, the variation in specific mass flow was significantly higher than that given by the ratio in channel width and the effect extended outside the channel. The velocity distribution around the blade obtained in the theoretical calculation compares very well with experimental values.

Lewis Flight Propulsion Laboratory,
National Advisory Committee for Aeronautics,
Cleveland, Ohio, February 5, 1951.

APPENDIX - DERIVATION OF EQUATIONS

If the fluid flow in turbomachines can be assumed to occur on surfaces of revolution, it may be analyzed on a two-dimensional basis with the flow passing through a number of stream filaments of revolution (fig. 1(a)), the thickness of which may be taken as that obtained in a through-flow calculation (reference 22). Such flow can be most conveniently described by a set of orthogonal coordinates l and φ, where l is the arc length of the generating line of the mean surface of revolution in the meridional plane, and φ is the angle (fig. 1(b)). When the flow across an element defined by dl and $d\varphi$ is considered (fig. 1(c)), the continuity relation for steady relative flow gives

$$\rho W_l \tau r d\varphi + \rho W_\varphi \left(\tau + \frac{1}{2}\frac{d\tau}{dl} dl\right) dl -$$

$$\left(\rho W_l + \frac{\partial(\rho W_l)}{\partial l} dl\right)\left(r + \sin\sigma\, dl\right)\left(\tau + \frac{d\tau}{dl} dl\right) d\varphi -$$

$$\left(\rho W_\varphi + \frac{\partial(\rho W_\varphi)}{\partial \varphi} d\varphi\right)\left(\tau + \frac{1}{2}\frac{d\tau}{dl} dl\right) dl = 0$$

Factoring out $d\varphi\, dl$ and allowing $d\varphi$ and dl to approach zero in the factor yield

$$-\rho W_l r \frac{d\tau}{dl} - r\tau \frac{\partial(\rho W_l)}{\partial l} - \rho W_l \tau \sin\sigma - \tau \frac{\partial(\rho W_\varphi)}{\partial \varphi} = 0 \qquad (A1)$$

By the use of the relation

$$\frac{dr}{dl} = \sin\sigma \qquad (A2)$$

equation (A1) can be written as

$$\frac{\partial(\tau \rho W_l r)}{\partial l} + \frac{\partial(\tau \rho W_\varphi)}{\partial \varphi} = 0 \qquad (1)$$

For steady adiabatic frictionless flow with uniform inlet conditions, the equation of motion in the circumferential direction can be obtained from equation (14a) of reference 22 as

$$\frac{1}{r}\left\{\frac{\partial W_l}{\partial \varphi} - \frac{\partial}{\partial l}\left[r(W_\varphi + \omega r)\right]\right\} = 0$$

or

$$\frac{1}{r}\frac{\partial W_l}{\partial \varphi} - \frac{\partial W_\varphi}{\partial l} - \frac{W_\varphi \sin \sigma}{r} - 2\omega \sin \sigma = 0 \qquad (2)$$

Special Case of Conical Surface

For the special case of two-dimensional flow between two neighboring surfaces of revolution, where the mean stream surface can be taken as the surface of a right circular cone whose axis coincides with the z-axis, σ becomes a constant. If l is measured from the apex of the cone,

$$r = l \sin \sigma$$

and equations (2) and (5) become, respectively,

$$\frac{1}{r}\frac{\partial W_l}{\partial \varphi} - \frac{\partial W_\varphi}{\partial l} - \frac{W_\varphi}{l} - 2\omega \sin \sigma = 0 \qquad (A4)$$

and

$$\frac{\partial^2 \psi}{\partial l^2} + \left(\frac{1}{l} - \frac{\partial \ln T}{\partial l}\right)\frac{\partial \psi}{\partial l} + \frac{1}{r^2}\frac{\partial^2 \psi}{\partial \varphi^2} -$$

$$\left(\frac{\partial \ln \rho}{\partial l}\frac{\partial \psi}{\partial l} + \frac{1}{r^2}\frac{\partial \ln \rho}{\partial \varphi}\frac{\partial \psi}{\partial \varphi} + 2\omega\rho T \sin \sigma\right) = 0 \qquad (A5)$$

Alternative forms of equations (1) and the preceding two equations can be obtained in terms of l and an angle measured on the conical surface, as given in reference 17.

Special Case of Cylindrical Surface

For the special case of flow on a stream filament of revolution whose mean surface is a cylindrical surface, σ becomes zero, l becomes z, and equations (1), (2), (4), and (5) reduce to the following forms:

$$\frac{\partial(\tau\rho W_z)}{\partial z} + \frac{\partial(\tau\rho W_y)}{\partial y} = 0 \tag{A6}$$

$$\frac{\partial W_y}{\partial z} - \frac{\partial W_z}{\partial y} = 0 \tag{A7}$$

$$\left.\begin{aligned} \tau\rho W_z &= \frac{\partial\psi}{\partial y} \\ \tau\rho W_y &= -\frac{\partial\psi}{\partial z} \end{aligned}\right\} \tag{A8}$$

$$\frac{\partial^2\psi}{\partial z^2} - \frac{\partial \ln\tau}{\partial z}\frac{\partial\psi}{\partial z} + \frac{\partial^2\psi}{\partial y^2} - \left(\frac{\partial \ln\rho}{\partial z}\frac{\partial\psi}{\partial z} + \frac{\partial \ln\rho}{\partial y}\frac{\partial\psi}{\partial y}\right) = 0 \tag{A9}$$

where $y = r\varphi$ and r is a constant. When r is constant, the relation between density and ψ-derivatives is simplified to

$$\frac{\rho}{\rho_{T,i}} = \left[1 - \frac{\left(\frac{\partial\psi}{\partial z}\right)^2 + \left(\frac{\partial\psi}{\partial y}\right)^2}{2\,H_i\,\tau^2\rho^2}\right]^{\frac{1}{\gamma-1}} \tag{A10}$$

When the general table or graph constructed according to equation (7a) is used, Σ becomes simply $\left(\frac{\rho}{\rho_{T,i}}\right)^2$ and Φ becomes $\left[\left(\frac{\partial\psi}{\partial z}\right)^2 + \left(\frac{\partial\psi}{\partial y}\right)^2\right]$ $(2\,H_i\,\tau^2\rho_{T,i}{}^2)^{-1}$.

REFERENCES

1. Tyler, R. A.: The Available Theoretical Analyses of Two-Dimensional Cascade Flow. Aero. Note MT-4, Div. Mech. Eng., Nat. Res. Council Canada, 1948.

2. Traupel, W.: Calculation of Potential Flow through Blade Grids. Sulzer Tech. Rev., No. 1, 1945, pp. 25-42.

3. Vazsonyi, Andrew: On the Aerodynamic Design of Axial-Flow Compressors and Turbines. Jour. Appl. Mech., vol. 15, no. 1, March 1948, pp. 53-64.

4. Ferrari, Carle: Sulla determinazione del flusso attraverso ad una schiera di profili alari con forte curvatura. Aerotechnica. 28, 119-135 (1948).

5. Bugaenko, G. A.: On the Problem of Gas Flow over an Infinite Cascade Using Chaplygin's Approximation. NACA TM 1298, 1951.

6. Woolard, Henry W.: A Note on the Subsonic Compressible Flow about Airfoils in a Cascade. Jour. Aero. Sci., vol. 17, no. 6, June 1950, pp. 379-381.

7. Stodola, A.: Steam and Gas Turbines. Vol. II. McGraw-Hill Book Co., Inc., 1927, pp. 992-994 and 998-1006. (Reprinted, Peter Smith (New York, 1945.)

8. Weinig, F.: Flow Patterns of a Compressible Gas through Turbine Cascades When Shock Waves are Avoided. Tech. Rep. No. F-TR-2141-ND, Air Materiel Command, AAF, May 1947.

9. Huppert, M. C., and MacGregor, Charles: Comparison between Predicted and Observed Performance of Gas-Turbine Stator Blade Designed for Free-Vortex Flow. NACA TN 1810, 1949.

10. Poritsky, H., Sells, B. E., and Danforth, C. E.: Graphical, Mechanical, and Electrical Aids for Compressible Fluid Flow. Jour. Appl. Mech., vol. 17, no. 1, March 1950, pp. 37-46.

11. Spannhake, W.: Anwendung der konformen Abbildung auf die Berechnung von Strömungen in Kreiselrädern. Z.f.a.M.M., Bd. 5, Heft 6, Dez. 1925, S. 481-484.

12. Sörensen, E.: Potential Flow through Centrifugal Pumps and Turbines. NACA TM 973, 1941.

13. Busemann, A.: Das Förderhöhenverhältnis radialer Kreiselpumpen mit logarithmisch-spiraligen Schaufeln, Z.f.a.M.M., Bd. 8, Heft 5, Oct. 1928, S. 372.

14. Bollay, William: The Theory of Flow through Centrifugal Pumps. Theodore von Kármán Anniversary Vol., C.I.T., May 11, 1941, pp. 273-284.

15. Concordia, C., and Carter, G. K.: D-C Network-Analyzer Determination of Fluid-Flow Pattern in a Centrifugal Impeller. Jour. App. Mech., vol. 14, no. 2, June 1947, pp. A113-A118.

16. Sheets, H. E.: The Flow through Centrifugal Compressors and Pumps. ASME Trans., vol. 72, no. 7, Oct. 1950, pp. 1009-1015.

17. Stanitz, John D.: Two-Dimensional Compressible Flow in Turbomachines with Conic Flow Surfaces. NACA Rep. 935, 1949. (Formerely NACA TN 1744.)

18. Wu, Chung-Hua: Formulas and Tables of Coefficients for Numerical Differentiation with Function Values Given at Unequally Spaced Points and Application to Solution of Partial Differential Equations. NACA TN 2214, 1950.

19. Fox, L.: Some Improvements in the Use of Relaxation Methods for the Solution of Ordinary and Partial Differential Equations. Proc. Roy. Soc. London, vol. 190, no. A1020, sec. A, June 17, 1947. pp. 31-59.

20. Southwell, R. V.: Relaxation Methods in Theoretical Physics. Clarendon Press (Oxford), 1946.

21. Emmons, Howard W.: Flow of a Compressible Fluid Past a Symmetrical Airfoil in a Wind Tunnel and in Free Air. NACA TN 1746, 1948.

22. Wu, Chung-Hua: A General Through-Flow Theory of Fluid Flow with Subsonic or Supersonic Velocity in Turbomachines of Arbitrary Hub and Casing Shapes. NACA TN 2302, 1951.

23. Bickley, W. G.: Formulae for Numerical Differentiation. The Math. Gazette, vol. XXV, no. 263, Feb. 1941, pp. 19-27.

24. Snyder, Frances E., and Livingston, Hubert M.: Coding of a Laplace Boundary Value Problem for the UNIVAC. Math. Tables and Other Aids to Computation, III, no. 25, Jan. 1949, pp. 341-350.

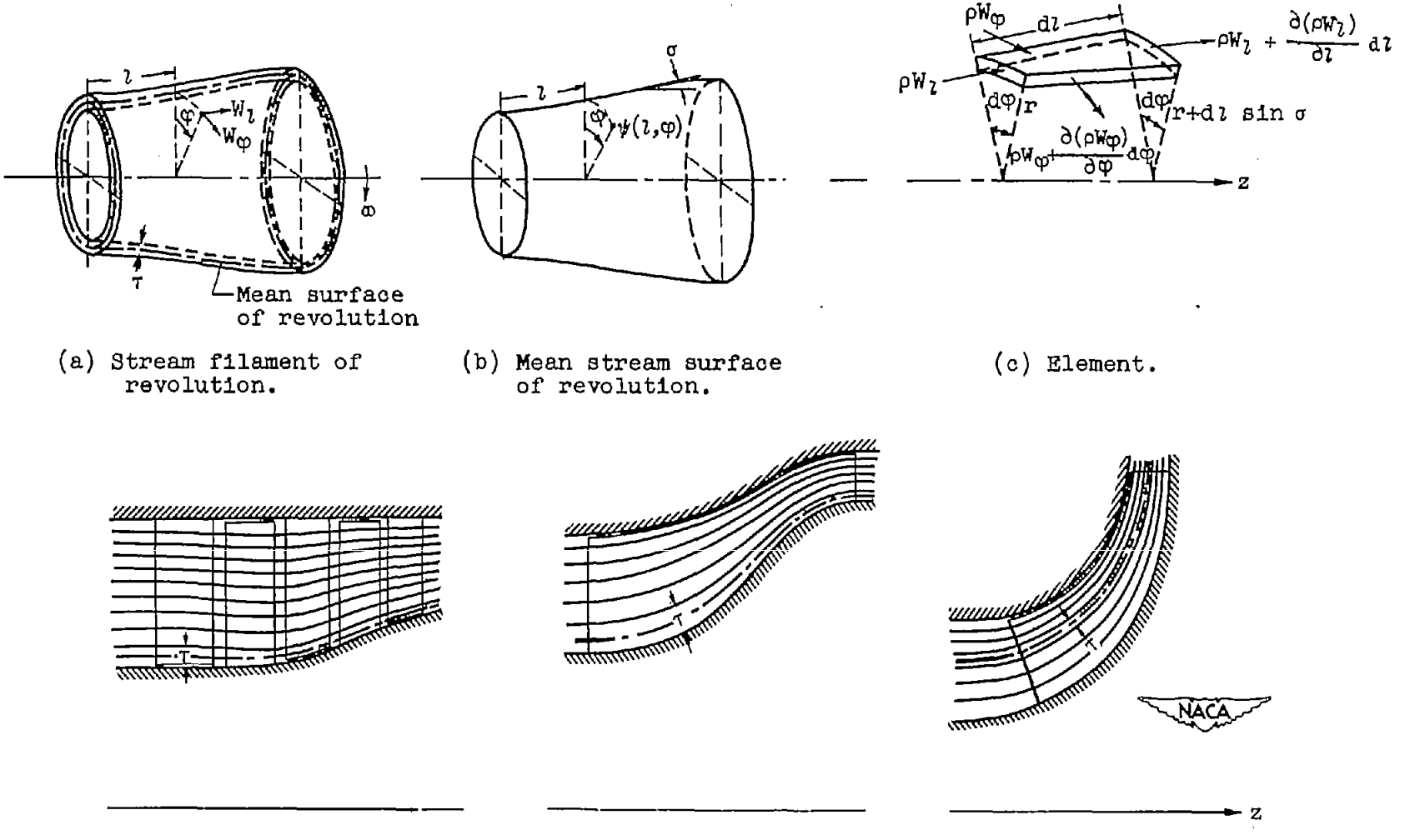

(a) Stream filament of revolution.

(b) Mean stream surface of revolution.

(c) Element.

(d) Applications to axial-flow, mixed-flow, and radial-flow turbomachines.

Figure 1. - Flow on arbitrary surface of revolution and stream filament of revolution.

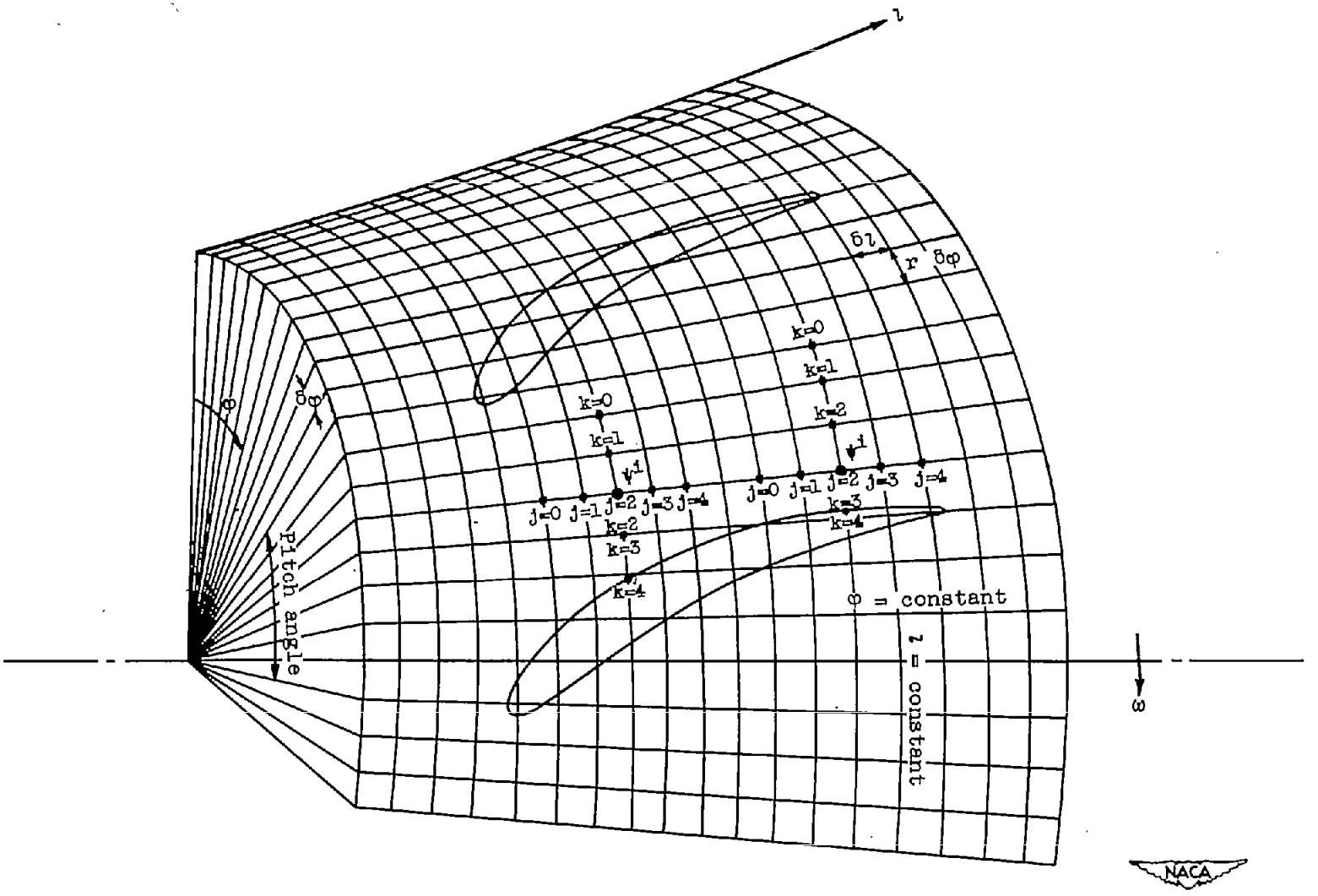

Figure 2. - Values of j and k for two grid points near boundary using five-point system.

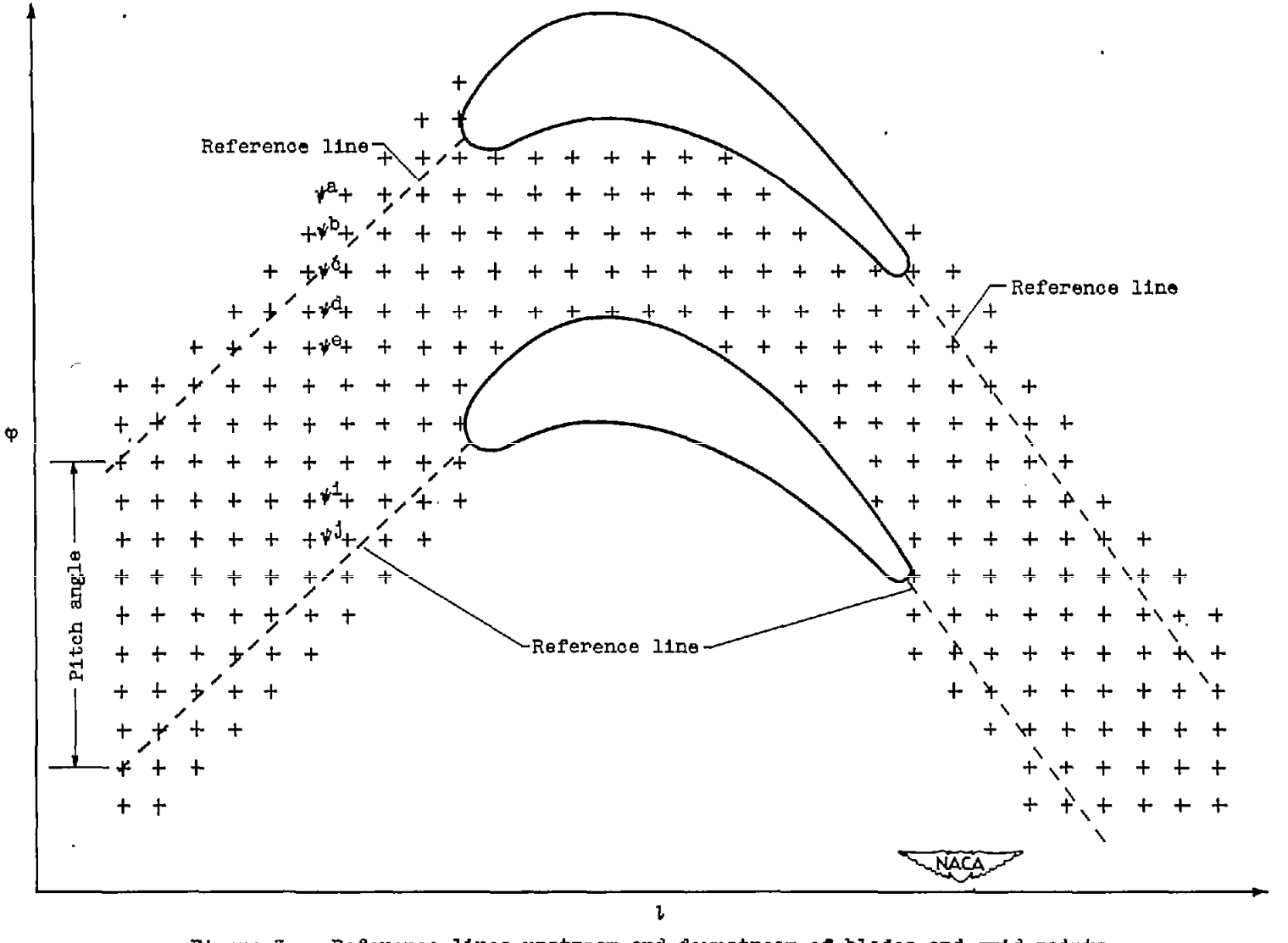

Figure 3. - Reference lines upstream and downstream of blades and grid points.

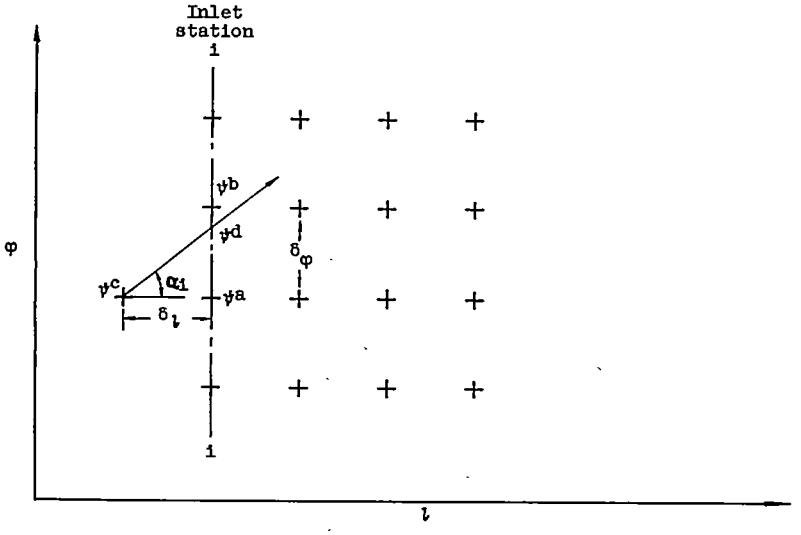

(a) Fixed-angle method.

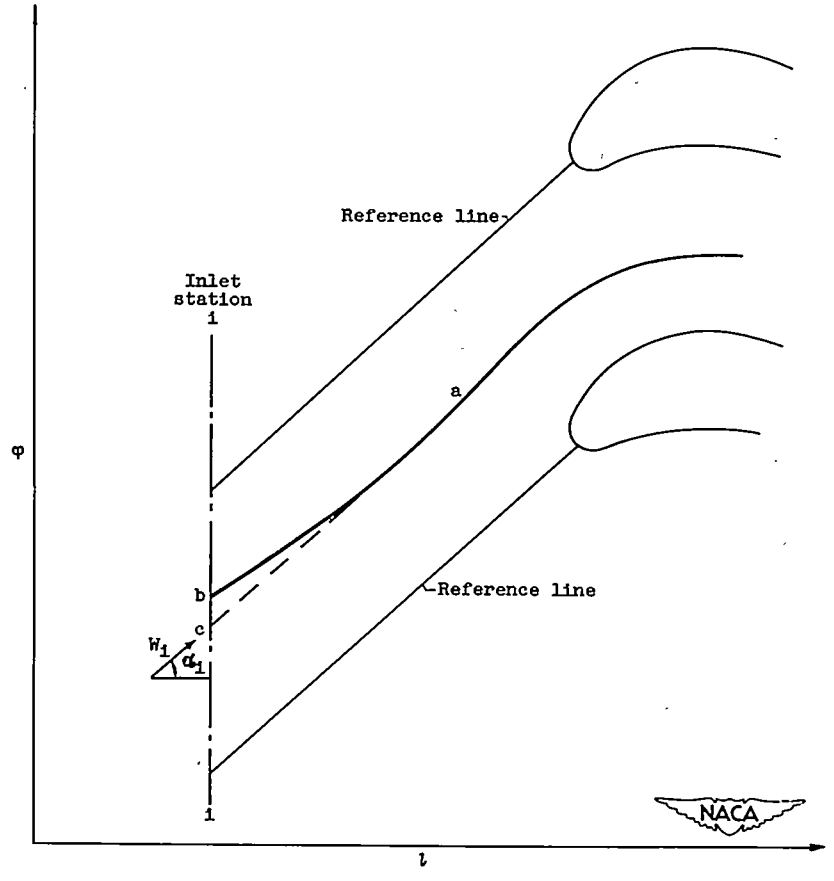

(b) Streamline-adjustment method.

Figure 4. - Treatment of inlet boundary condition.

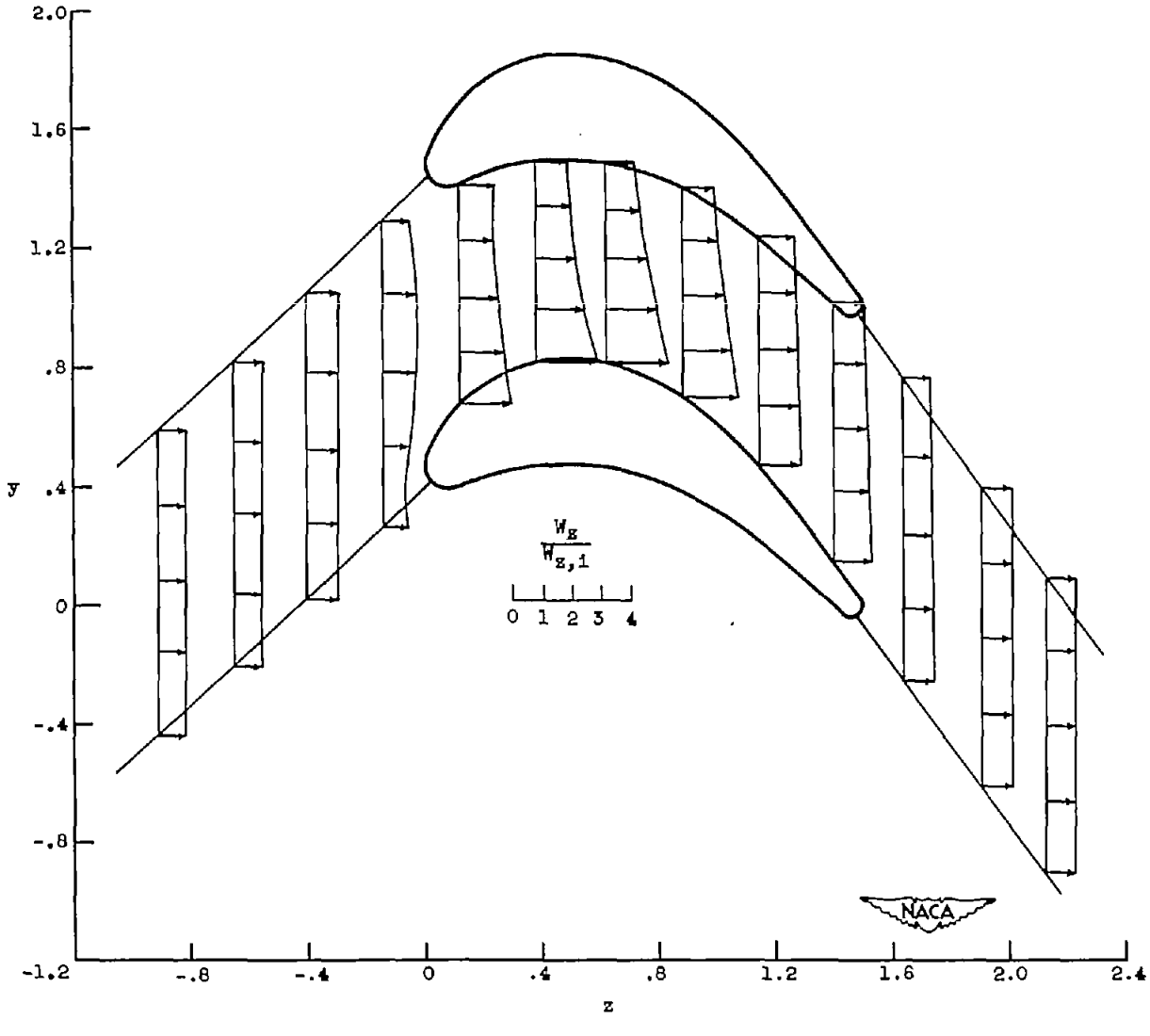

Figure 5. - Variation of axial velocity across channel for incompressible solution.

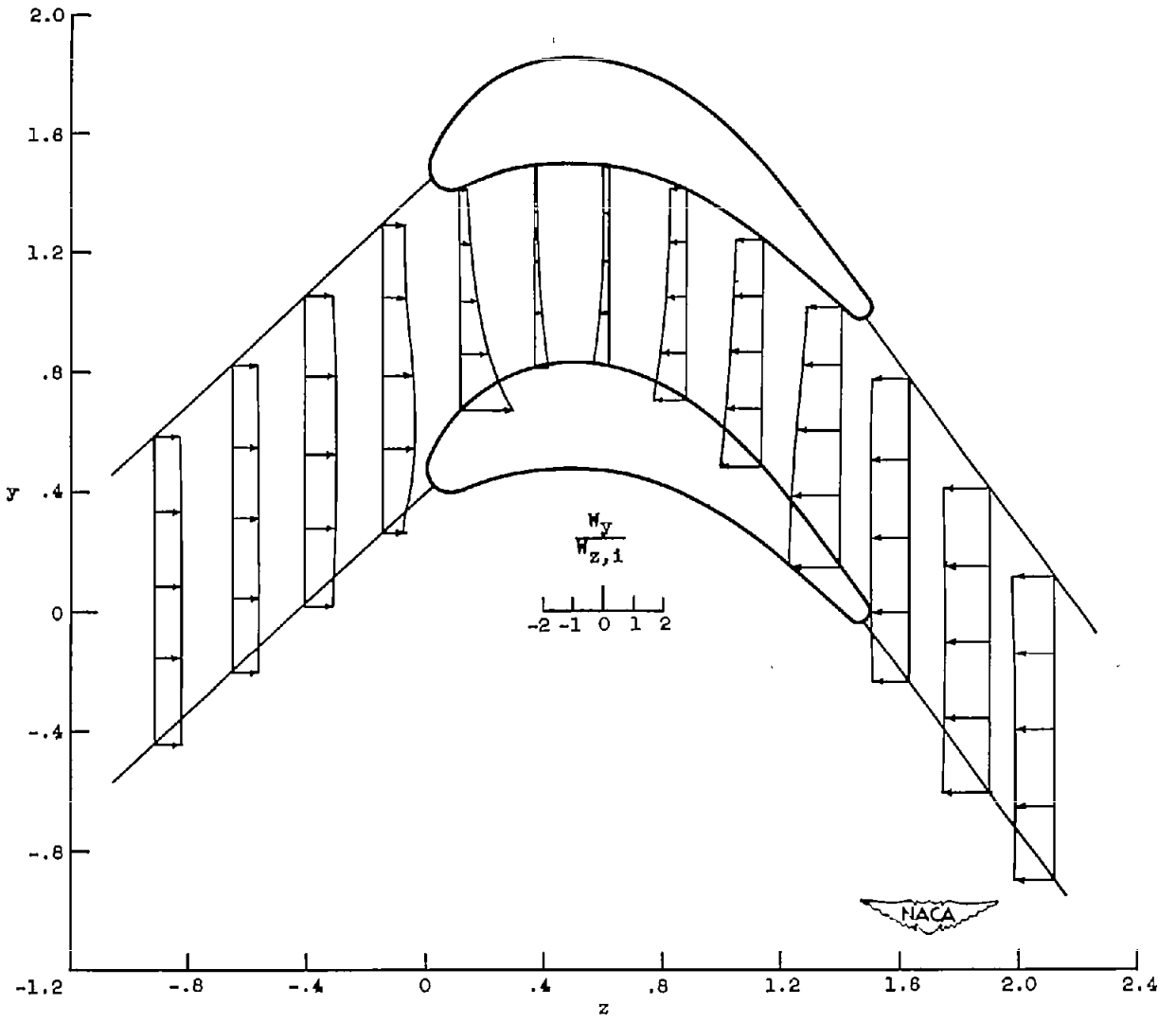

Figure 6. - Variation of magnitude of tangential velocity across channel for incompressible solution.

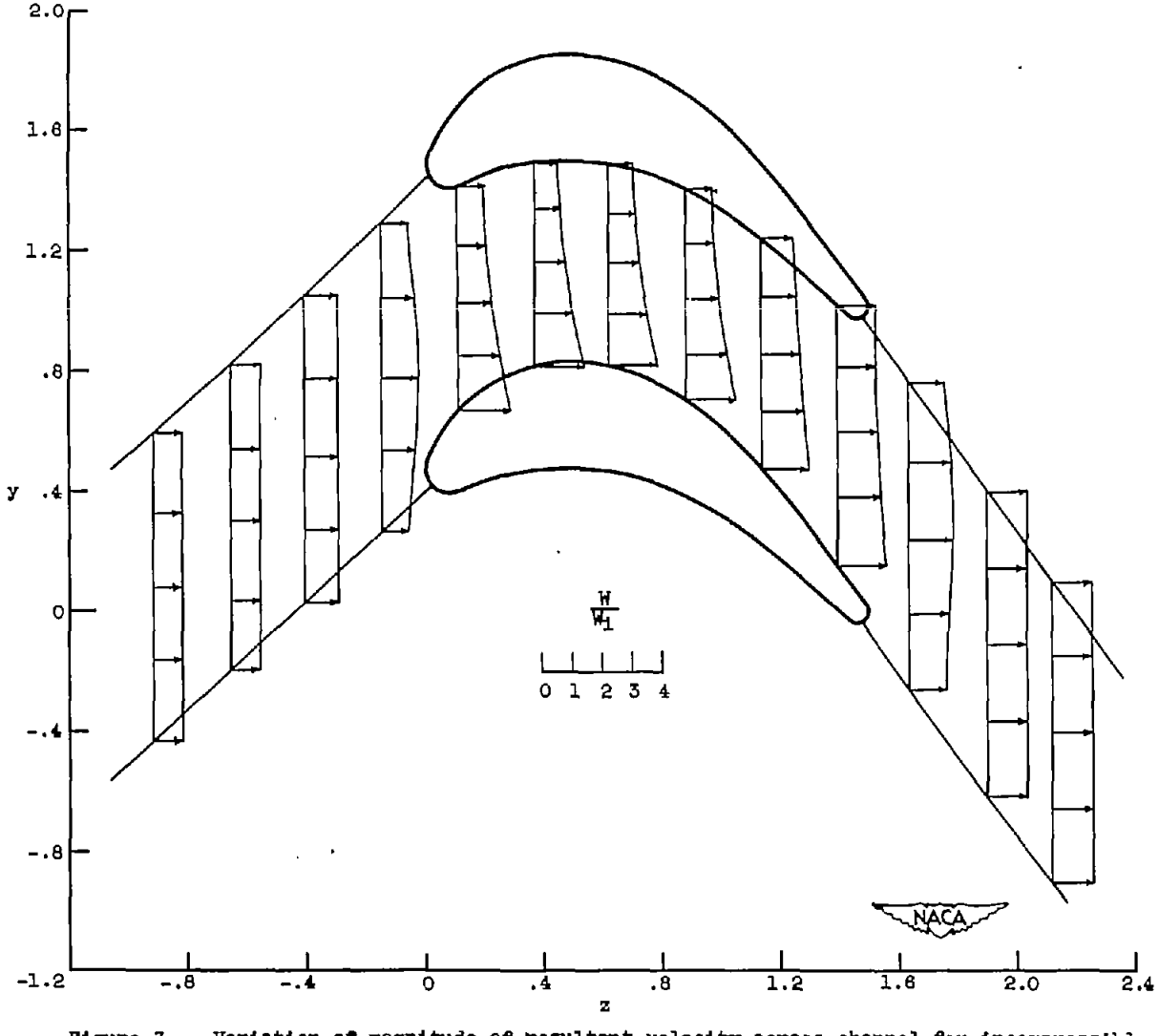

Figure 7. - Variation of magnitude of resultant velocity across channel for incompressible solution.

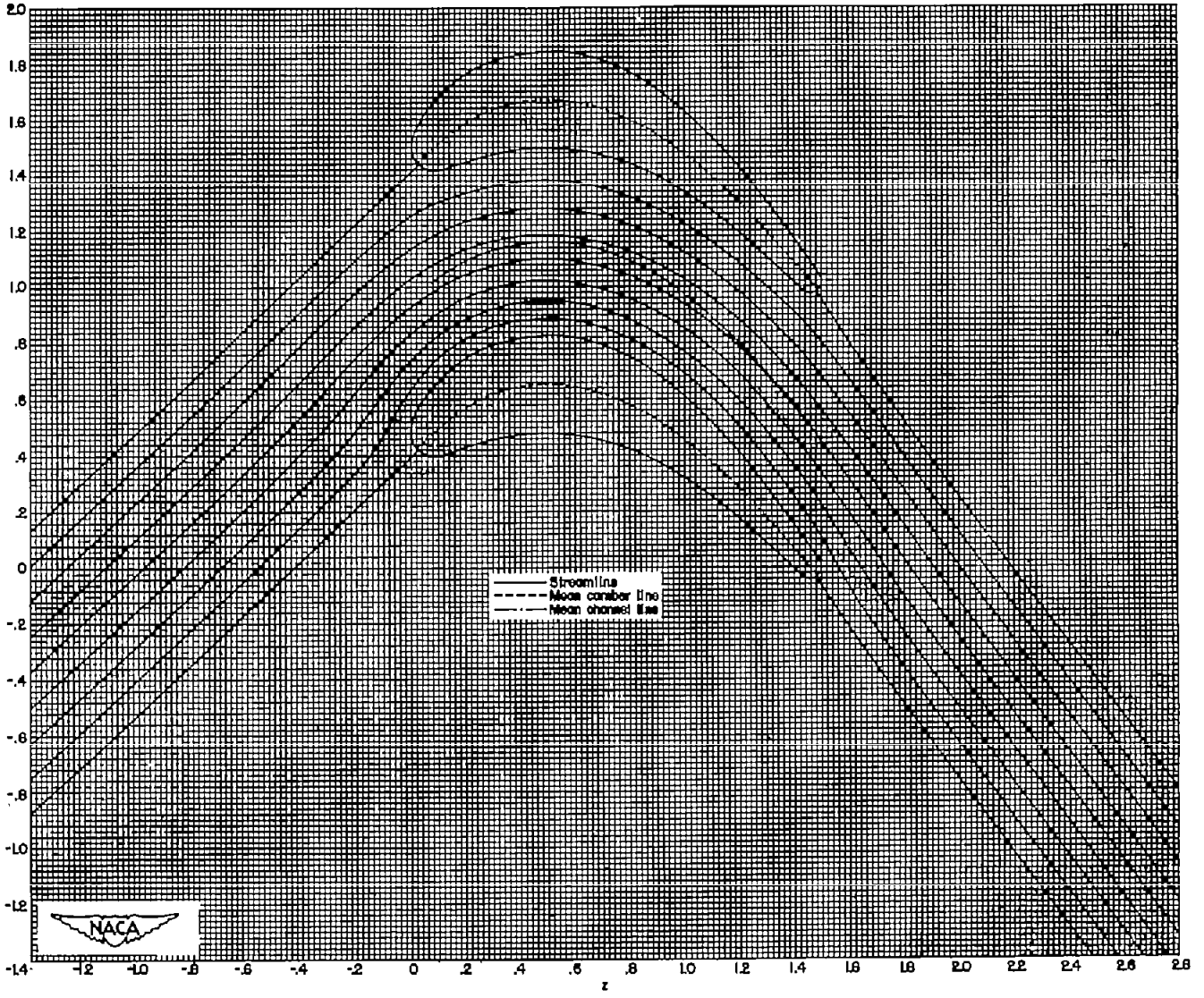

Figure 8. - Streamlines obtained in incompressible solution.

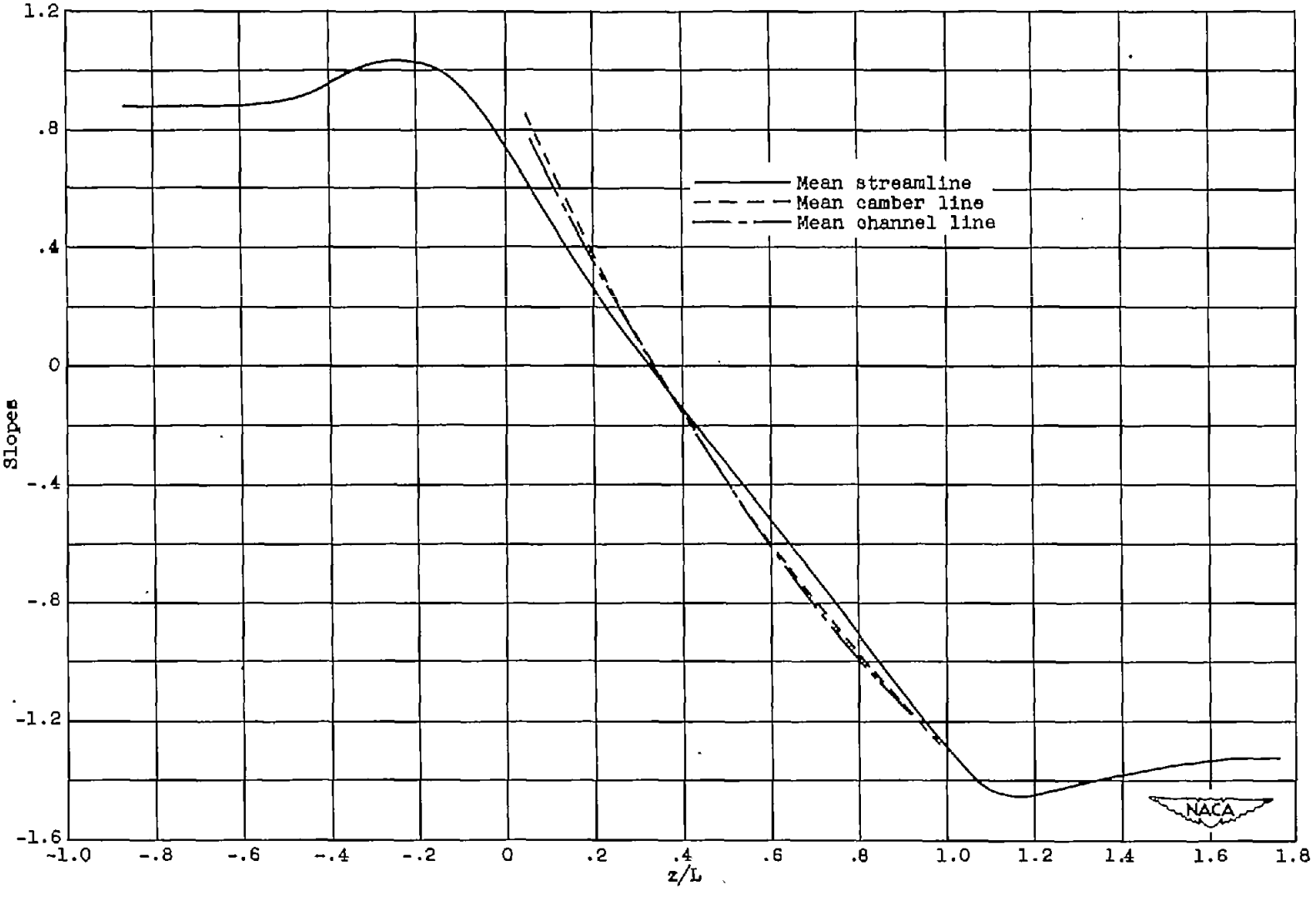

Figure 9. - Comparison of slopes of mean camber line, mean channel line, and mean streamline obtained in incompressible solution.

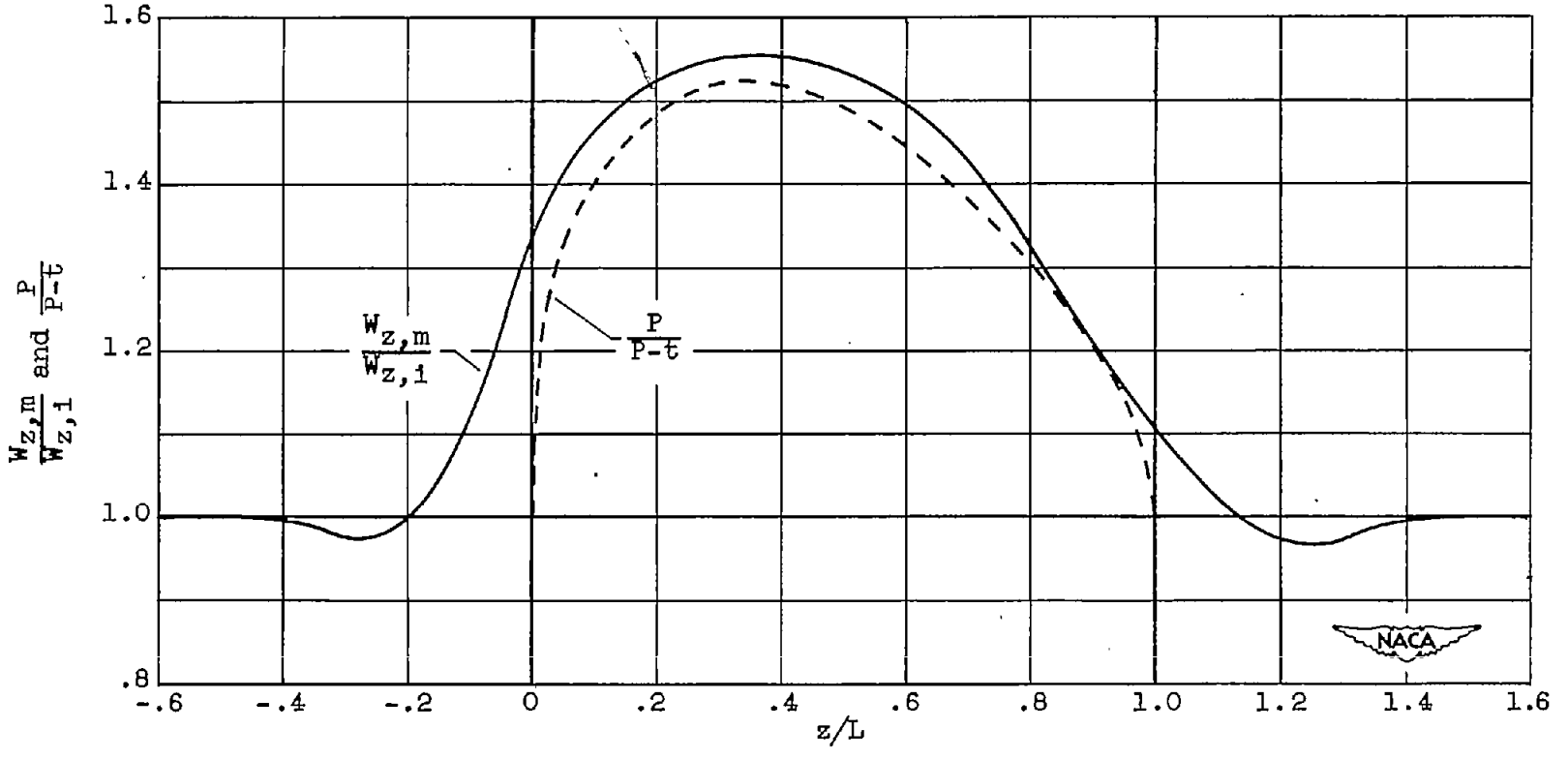

Figure 10. - Comparison between axial velocity along mean streamline and channel-width ratio for incompressible solution.

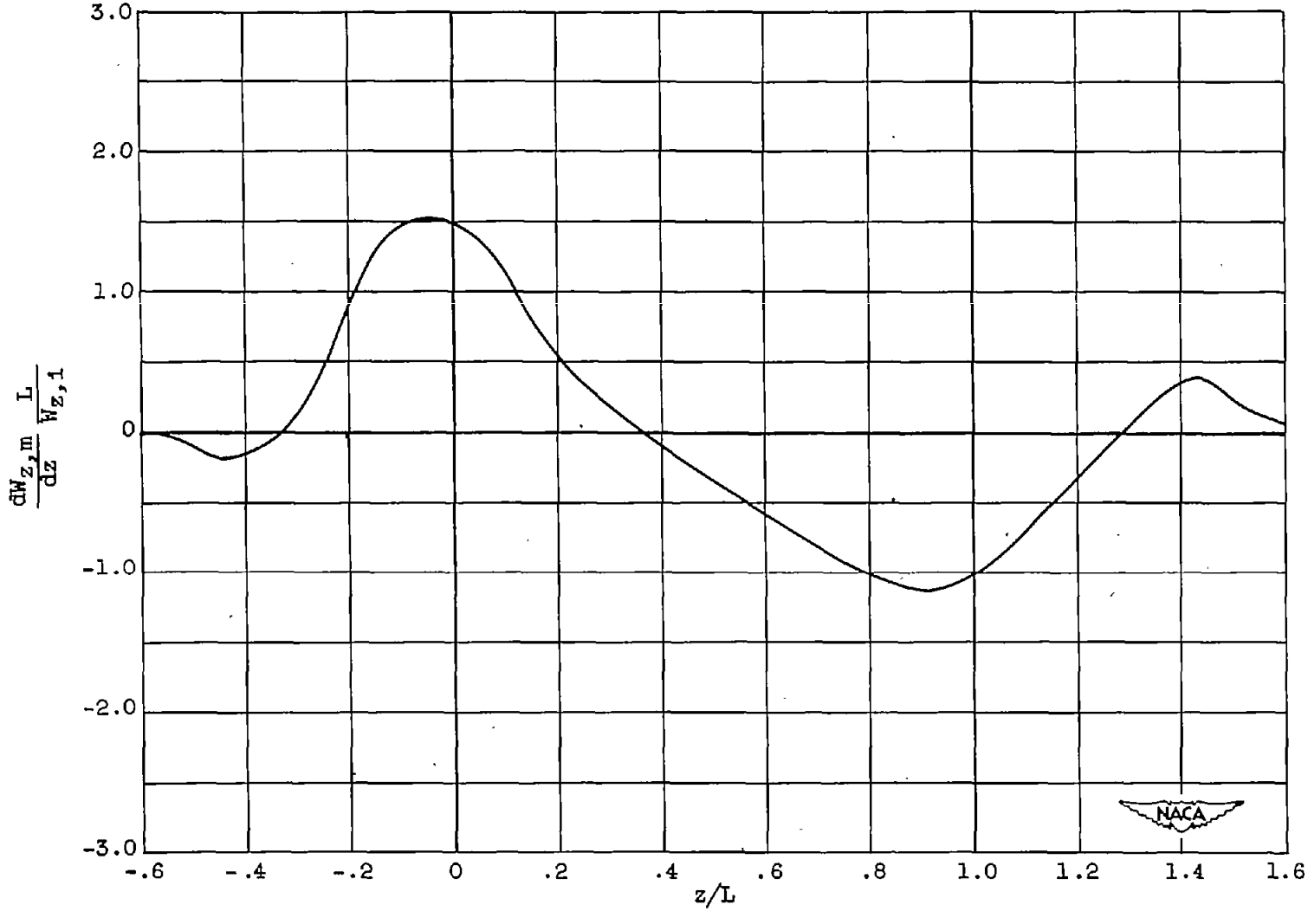

Figure 11. - Variation of total derivative of axial velocity on mean streamline with respect to axis for incompressible solution.

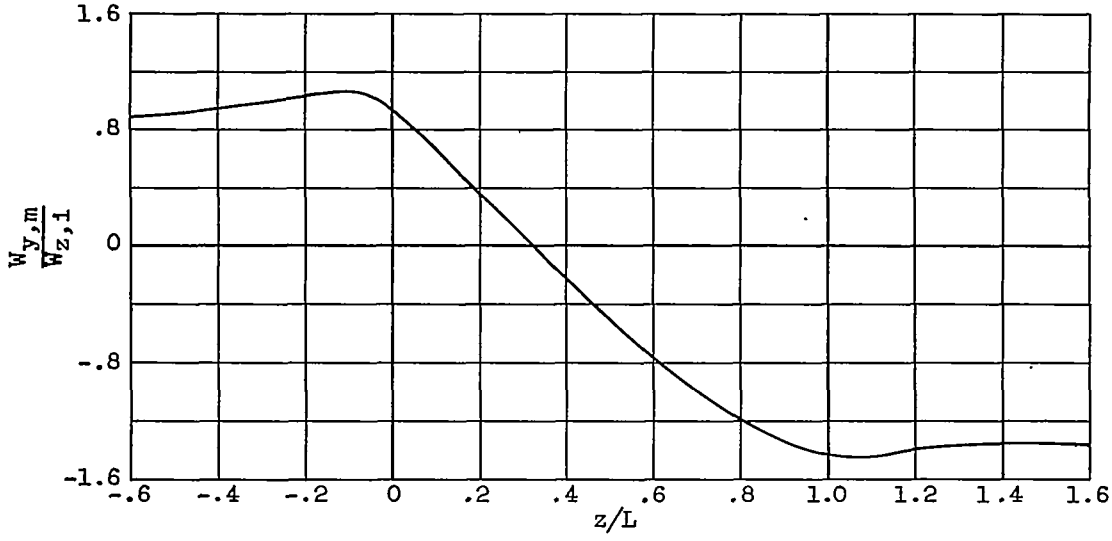

Figure 12. - Variation of tangential velocity on mean streamline with respect to axis for incompressible solution.

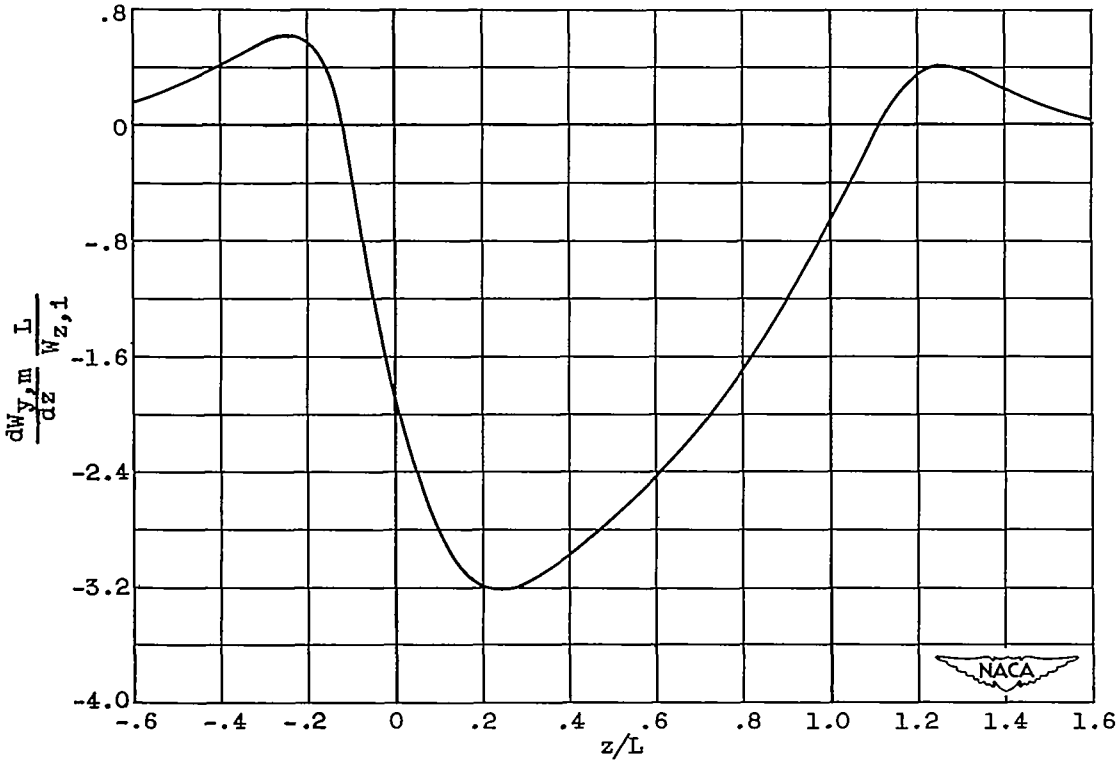

Figure 13. - Variation of total derivative of tangential velocity on mean streamline with respect to axis for incompressible solution.

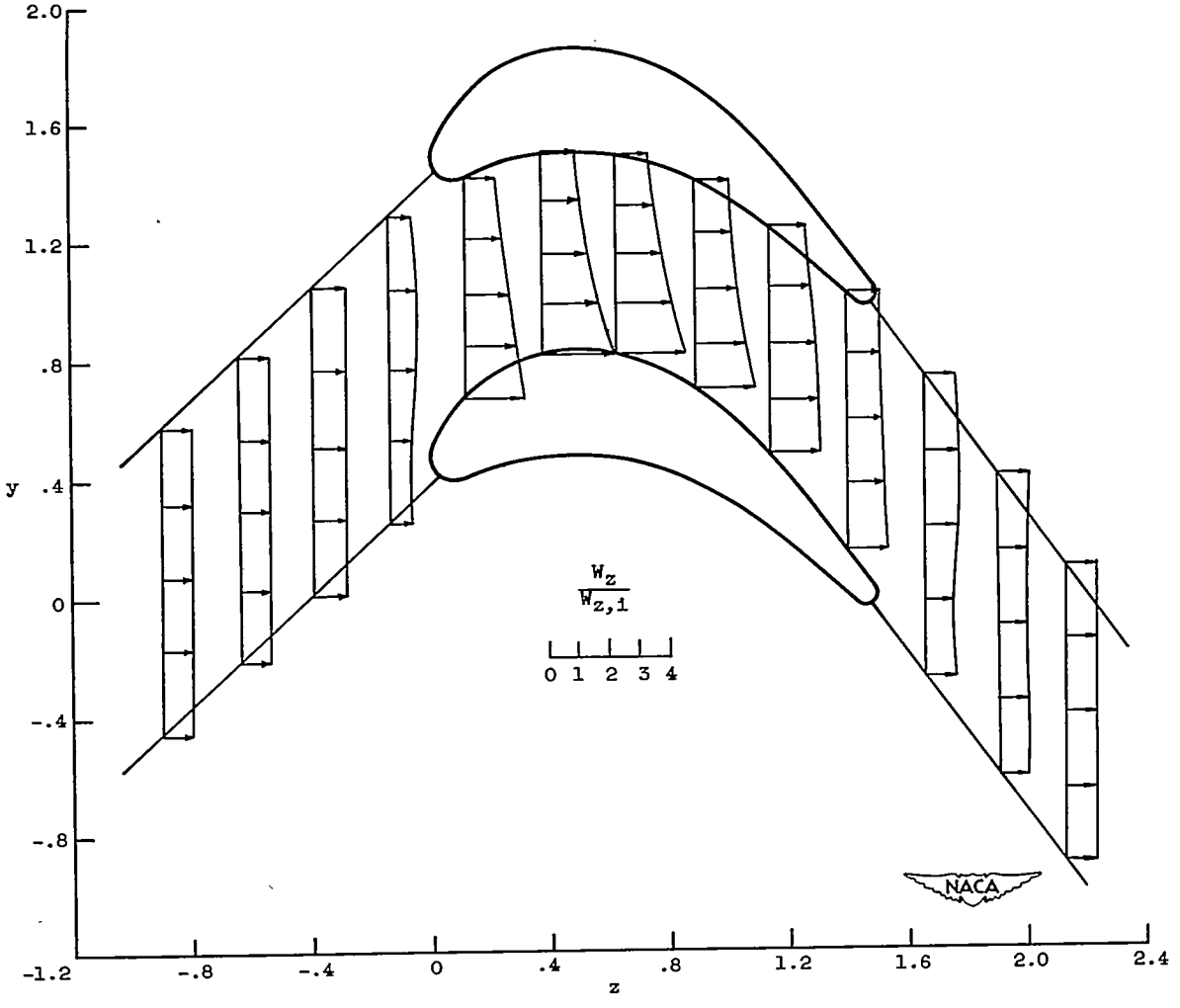

Figure 14. - Variation of axial velocity across channel for compressible solution. Inlet Mach number, 0.42.

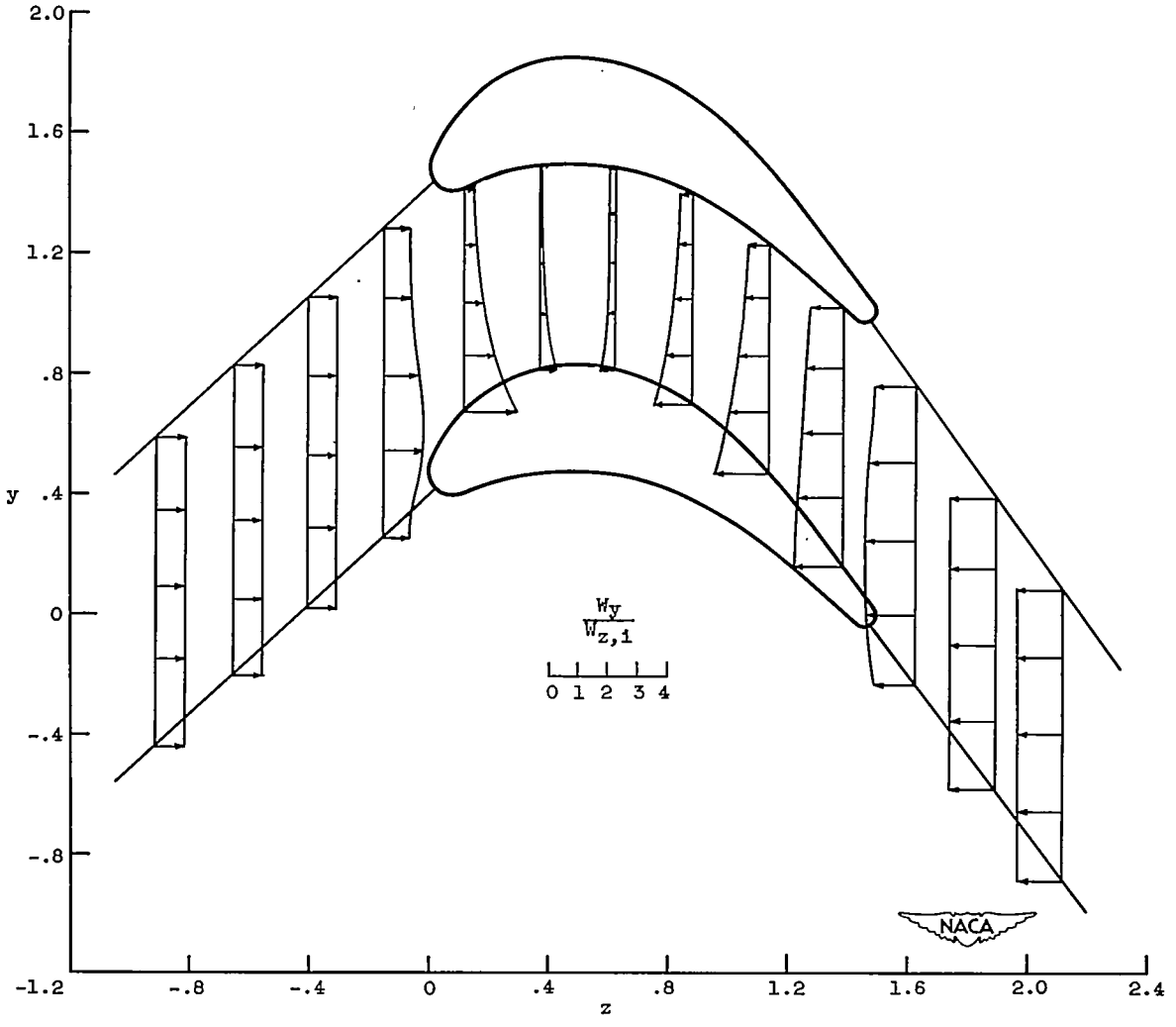

Figure 15. - Variation of magnitude of tangential velocity across channel for compressible solution. Inlet Mach number, 0.42.

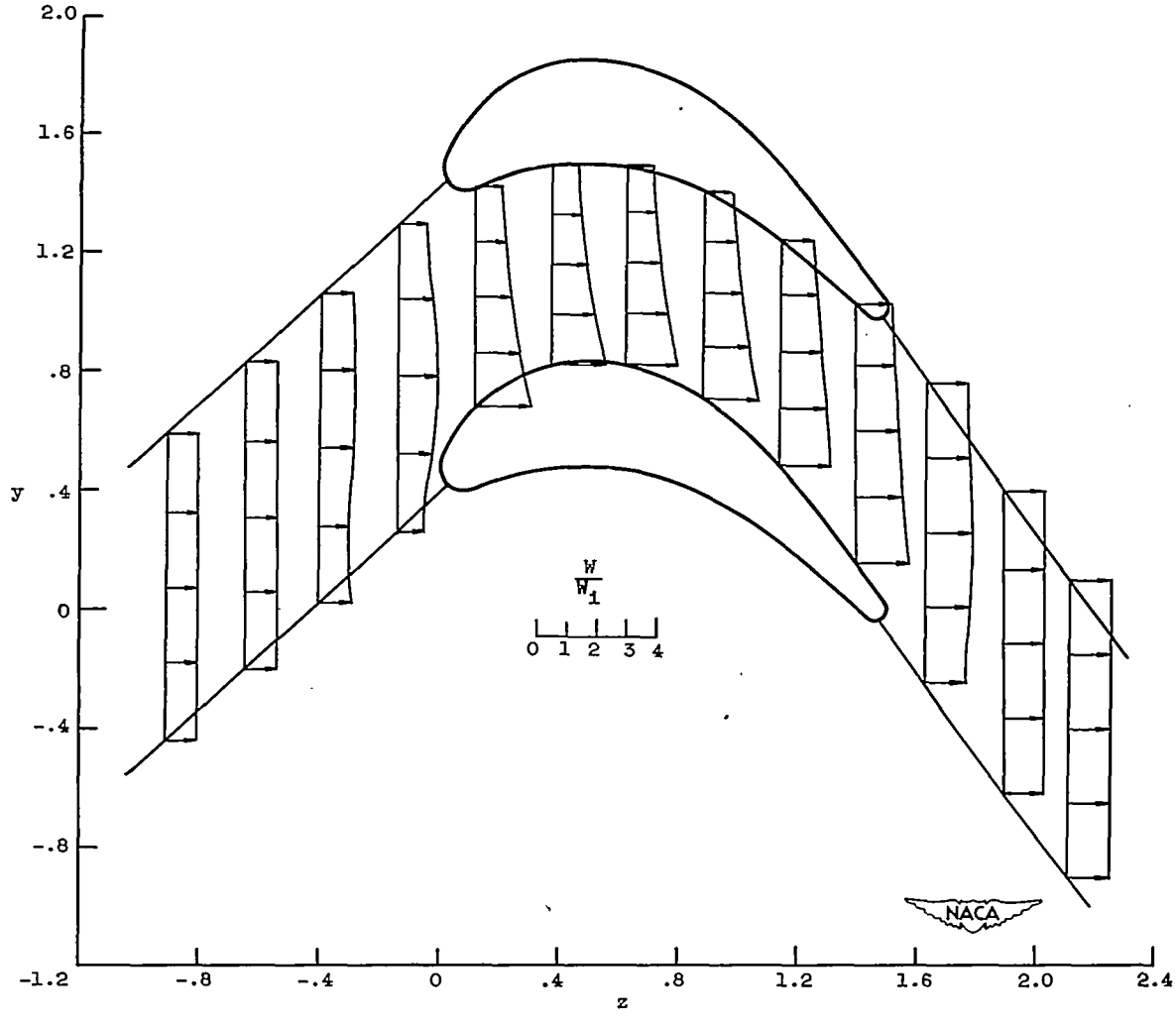

Figure 16. - Variation of magnitude of resultant velocity across channel for compressible solution. Inlet Mach number, 0.42.

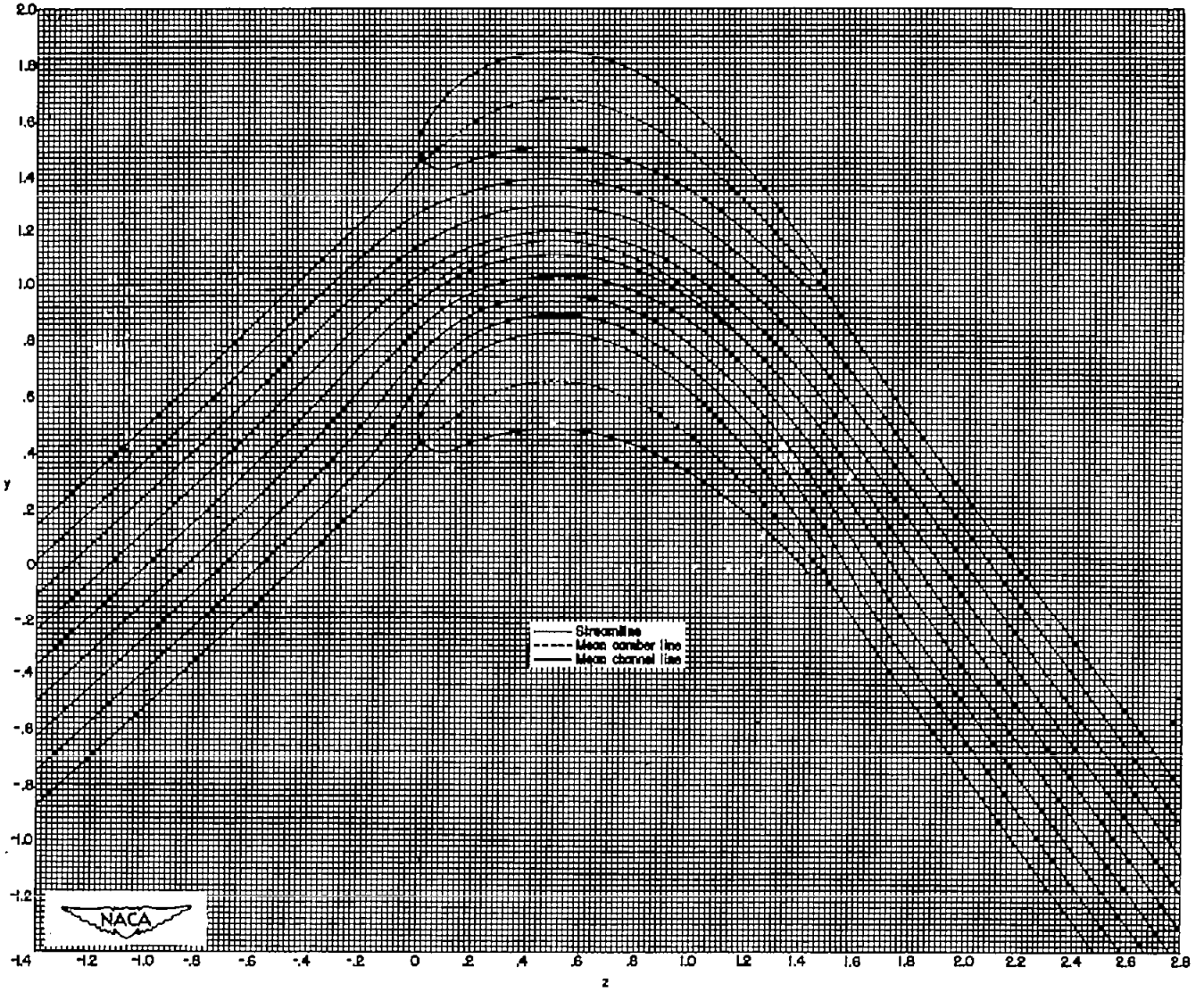

Figure 17. - Streamlines obtained in compressible solution. Inlet Mach number, 0.42.

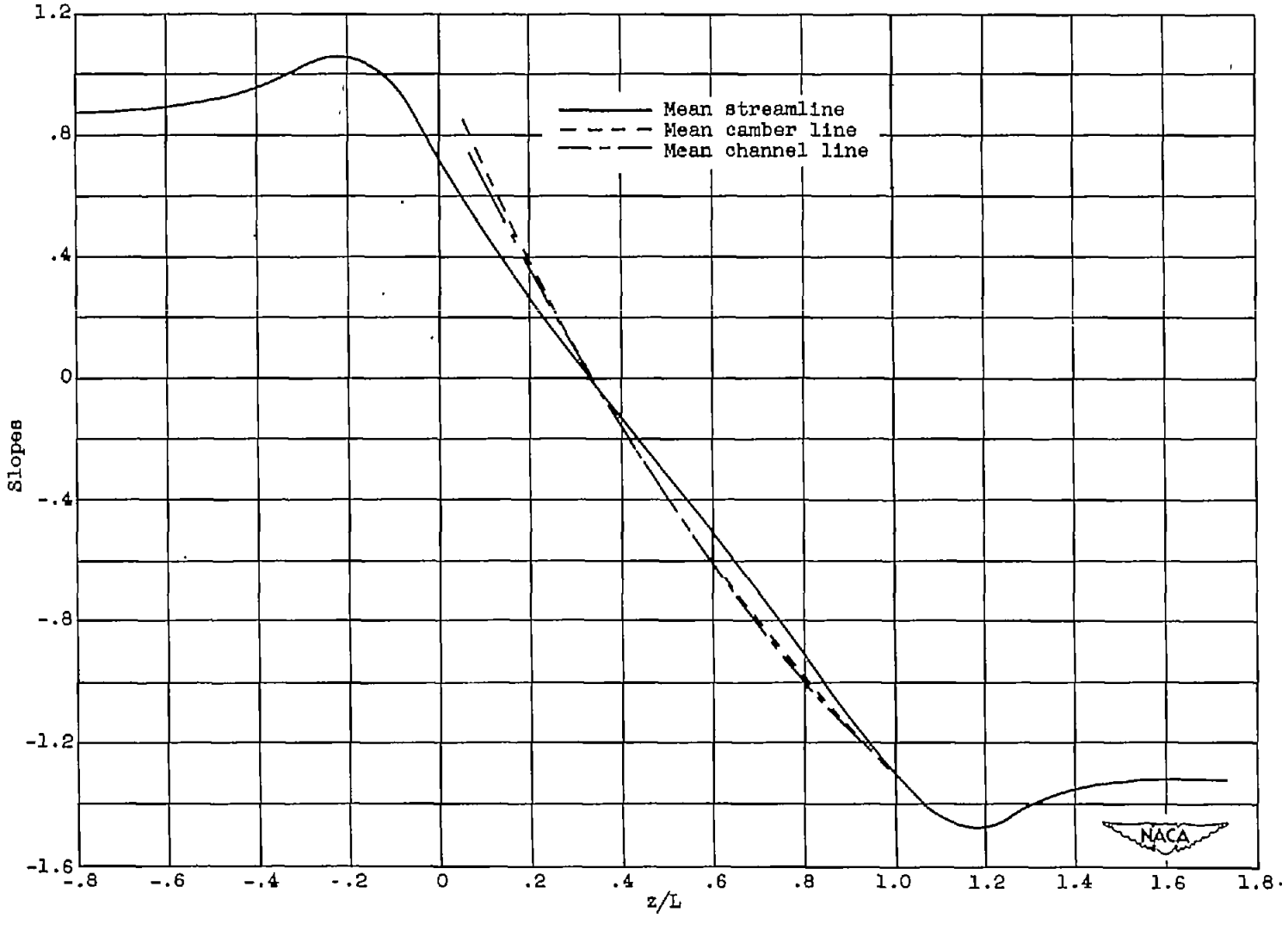

Figure 18. - Comparison of slopes of mean camber line, mean channel line, and mean streamline obtained in compressible solution. Inlet Mach number, 0.42.

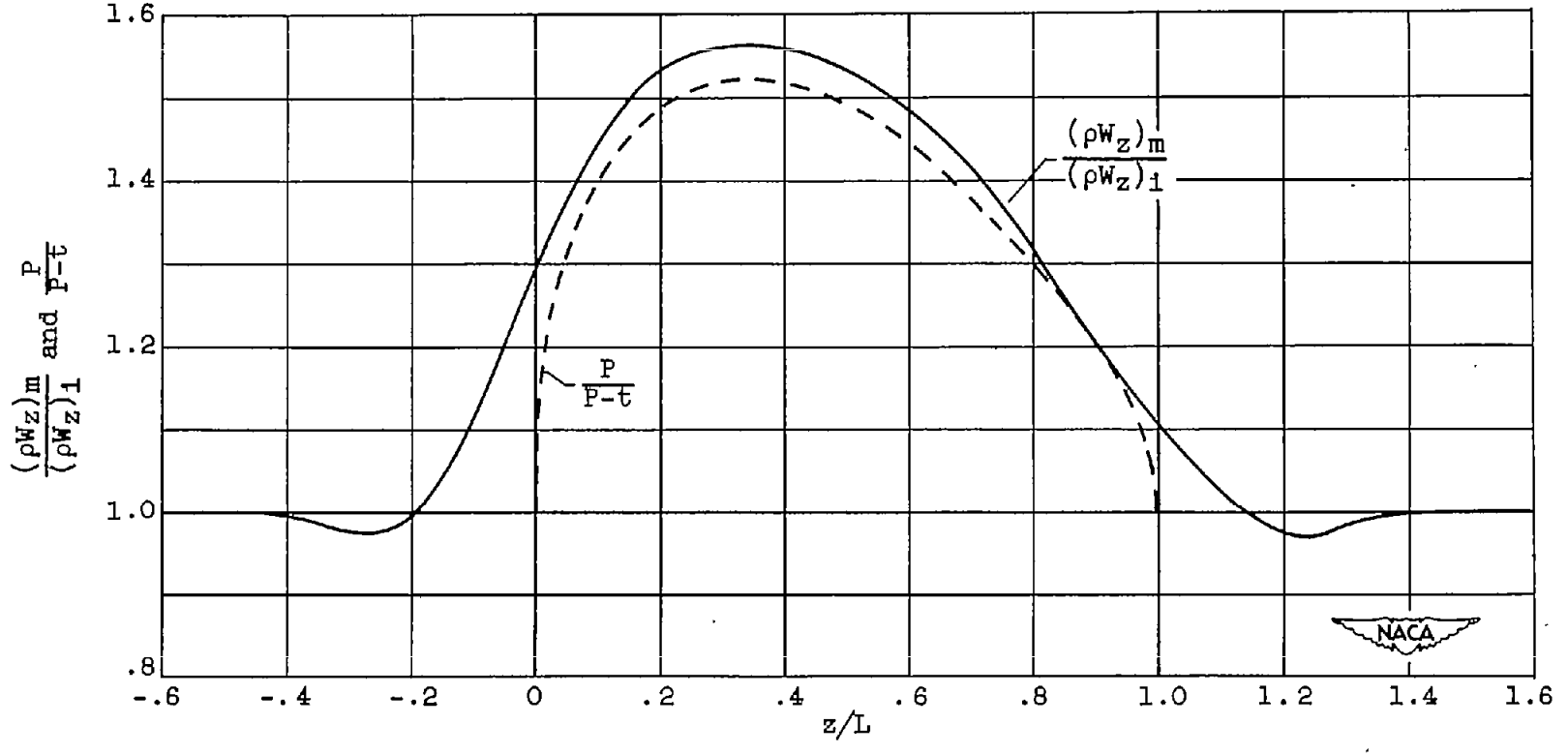

Figure 19. - Comparison between variation of specific mass flow along mean streamline in compressible flow and channel-width ratio. Inlet Mach number, 0.42.

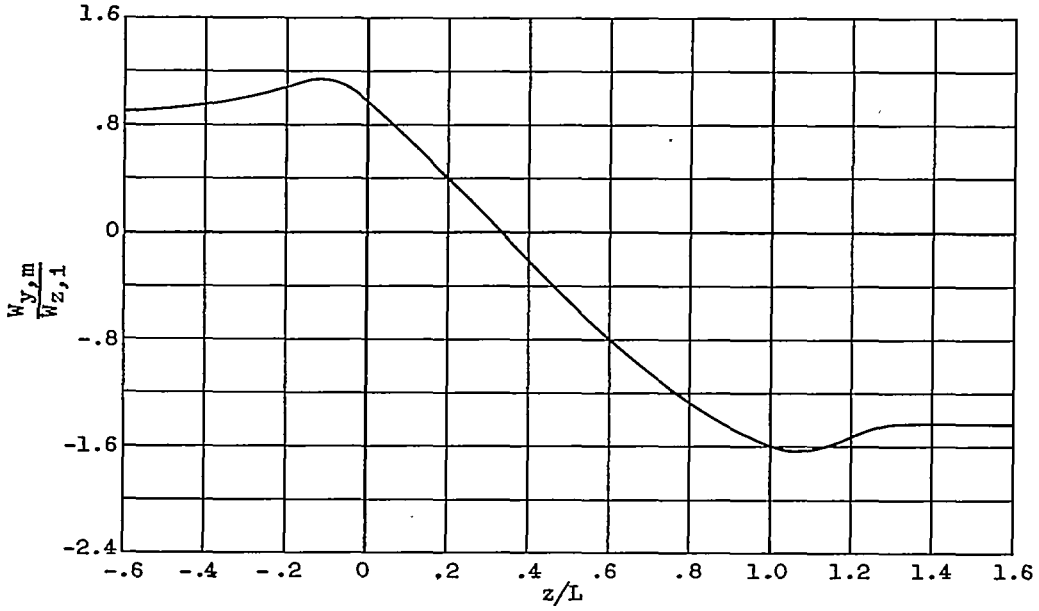

Figure 20. - Variation of tangential velocity on mean streamline with respect to axis for compressible solution. Inlet Mach number, 0.42.

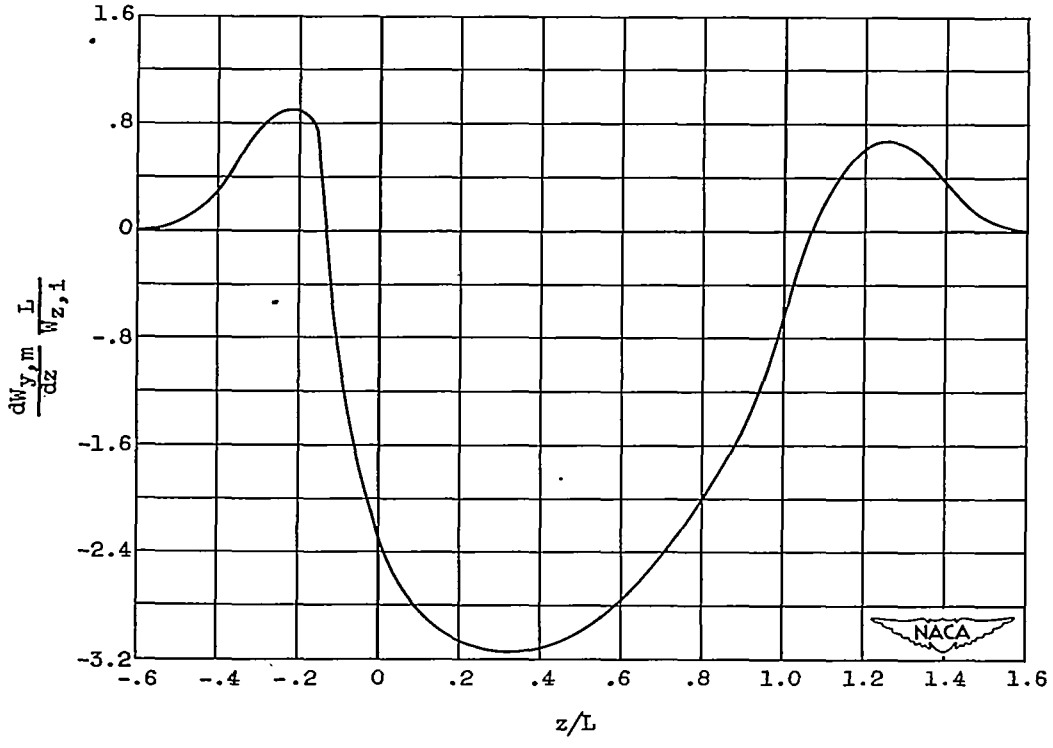

Figure 21. - Variation of total derivative of tangential velocity on mean streamline with respect to axis for compressible solution. Inlet Mach number, 0.42.

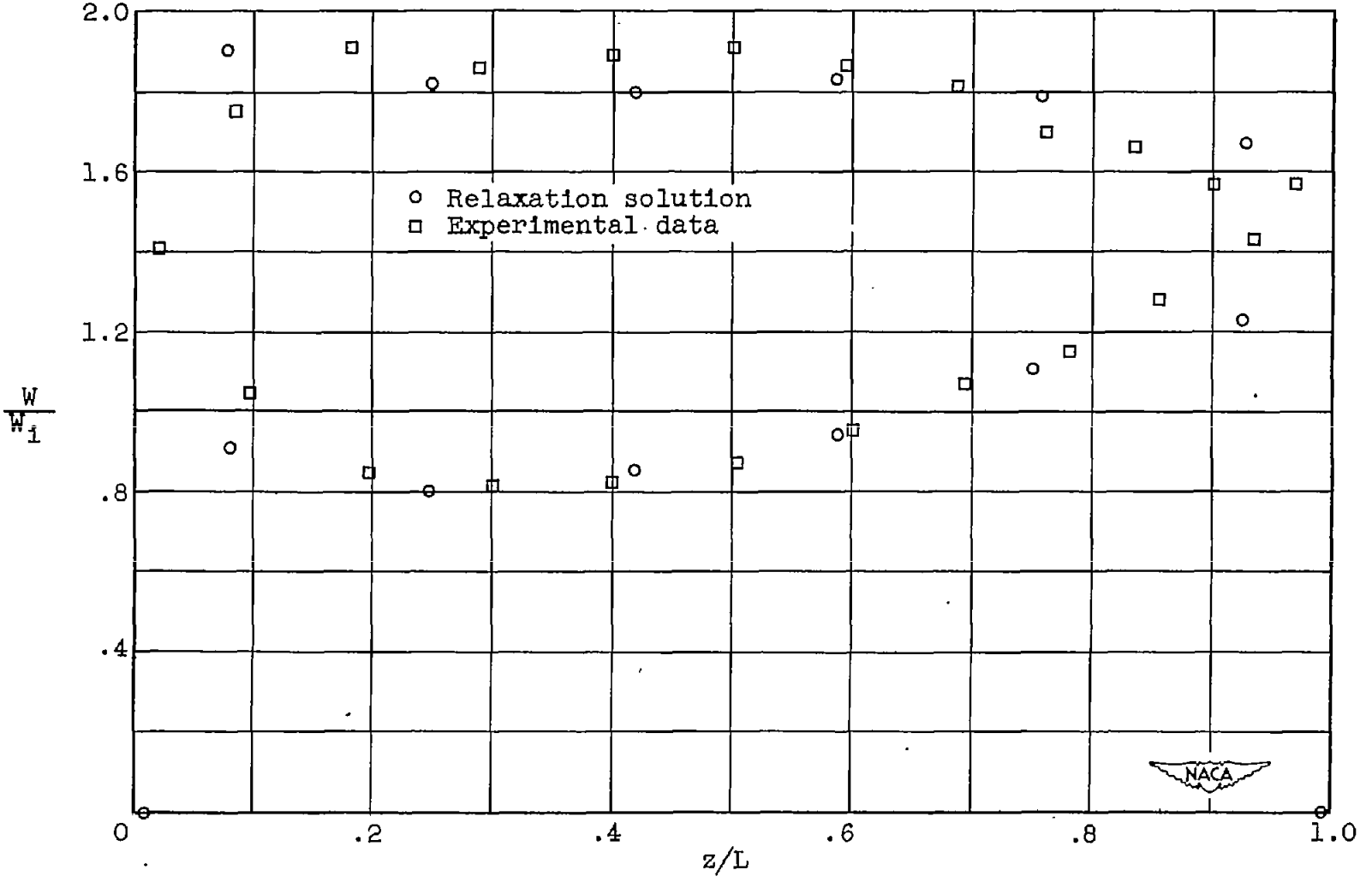

Figure 22. - Comparison of velocity distribution on blade obtained in numerical solution with experimental data. Inlet Mach number, 0.42.

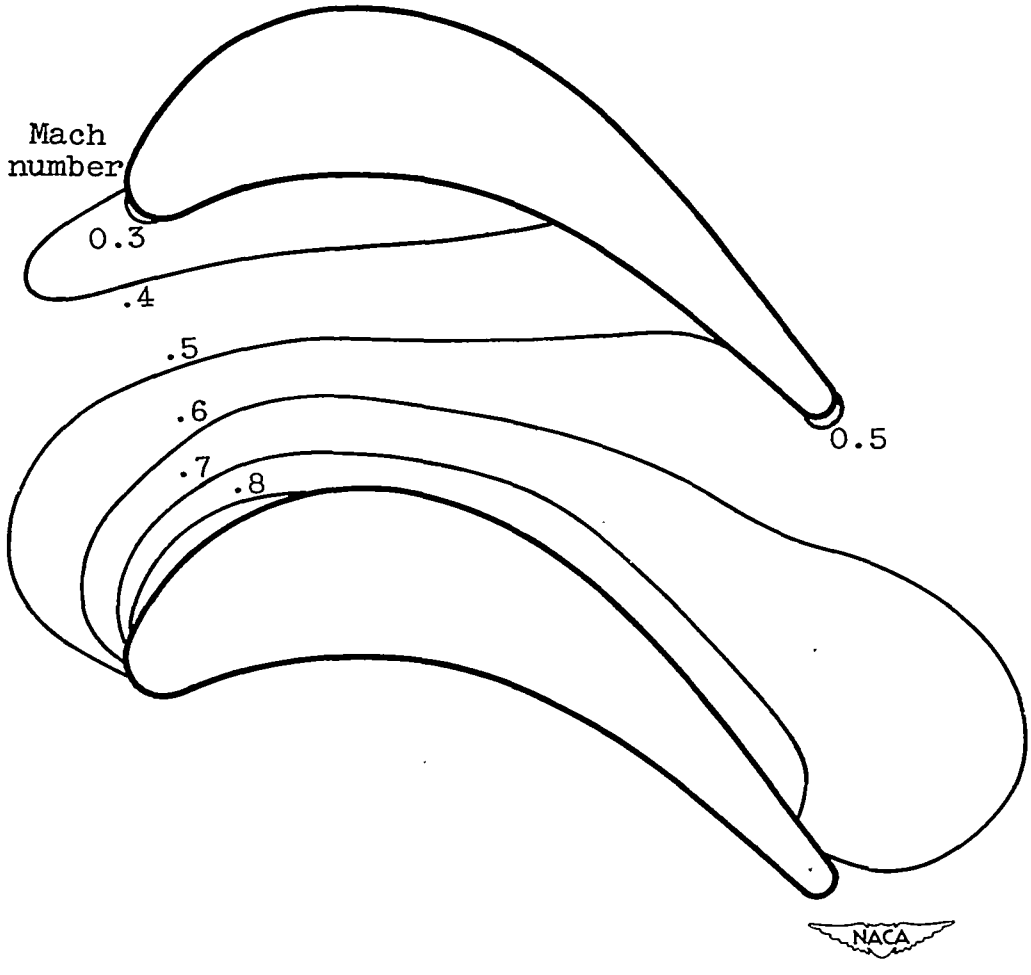

Figure 23. - Mach number contour as obtained in the relaxation solution. Inlet Mach number, 0.42; exit Mach number, 0.55.